ANALYSIS AND DESIGN OF CIRCULAR SHAFTS USING FINITE ELEMENT METHOD

by

Ali Saleh Chehadeh

A Thesis Presented to the Faculty of the
American University of Sharjah
College of Engineering
in Partial Fulfillment
of the Requirements
for the Degree of

Master of Science in
Civil Engineering

Sharjah, United Arab Emirates

June 2014

We, the undersigned, approve the Master's Thesis of Ali Saleh Chehadeh.
Thesis Title: Analysis and Design of Circular Shafts Using Finite Element Method

Signature	**Date of Signature** (dd/mm/yyyy)
_____	_____
Dr. Farid Abed Associate Professor Department of Civil Engineering Thesis Advisor	
_____	_____
Dr. Alper Turan Assistant Professor Department of Civil Engineering Thesis Co-Advisor	
_____	_____
Dr. Mousa Attom Professor Department of Civil Engineering Thesis Committee Member	
_____	_____
Dr. Basil Darras Assistant Professor Department of Mechanical Engineering Thesis Committee Member	
_____	_____
Dr. Ali Akan Head, Department of Civil Engineering	
_____	_____
Dr. Hany El Kadi Associate Dean, College of Engineering	
_____	_____
Dr. Leland Blank Dean, College of Engineering	
_____	_____
Dr. Khaled Assaleh Director of Graduate Studies	

Acknowledgements

In the name of Allah, the source of all knowledge, nothing could have ever been accomplished or come to existence without Allah's help.

I would like to express my appreciation to my advisors, Dr. Alper Turan for his great ideas, patience, kindness, and support throughout the research and Dr. Farid Abed for his great attitude, patience, and valuable help during the research period.

I would also like to thank my committee members, Dr. Mousa Attom and Dr. Basil Darras for their valuable suggestions and comments.

Dedication

To my parents

To my sisters and brothers

To my brothers in law

To my nephews and nieces

To my friends

To my wife to be

To anyone who reads, improves, or adds to this work

Abstract

Rapid expansion of urban areas has created a need to expand/rehabilitate the existing buried infrastructure at the same or a greater rate. Technical challenges such as variable soil and rock profiles, high groundwater tables, and limitations imposed by the built environment, combined with present fiscal and schedule limitations, necessitates the implementation of fast and cost effective construction methods. Since drilling procedures and equipment allow for the construction of overlapped pile systems in almost all subsurface conditions, secant pile walls have become a cost-effective shoring option. The secant pile walls constructed in a circular plan layout to form a vertical shaft provide unique advantages such as compression ring behavior. This thesis presents a parametric study to investigate the soil-structure interaction and mechanical response of circular shafts under different loading and boundary conditions using the finite element method. The aspects that were studied included the identification of earth pressure distributions exerted on circular shafts, the impact of excavation of single and multiple holes on the shaft stresses, the stresses in the shaft in cases of sloping bedrock, and the distribution of surcharge pressures on the shaft walls. The results showed that the earth pressures acting on the exterior surfaces of the shaft wall remained between active and at-rest values. The earth pressures can be represented by active distribution at shallow depths and at-rest distribution at larger depths. The results also indicated that the horizontal extent of the spread of surcharge induced lateral pressures around the shaft was significantly influenced by the type of soil as well as the width of the surcharge. It was noticed that the theoretical estimates of pressures underestimated the simulated values at larger depths. The sloping bedrock was also seen to result in significant deviations from the compression ring behavior. A large increase in the maximum compressive stresses and an emergence of some significant tensile stress zones were observed for bedrock inclinations larger than 20 degrees. The results presented in this study address various practical design concerns and should be of interest to those involved in the design and construction of vertical shafts.

Keywords: Diaphragm Wall, Compression Ring, Soil-Structure Interaction, Circular Shaft, Hole Excavation, Sloping Bedrock, Surcharge Effects

Table of Contents

List of Figures

List of Tables

Nomenclature

D	Shaft Diameter
R	Shaft Radius
r	Excavated Hole radius
t	Shaft Thickness
H	Shaft Height
$\emptyset$	Soil Friction Angle
A	Rock Layer Inclination Angle (˚)
q	Surcharge Uniform Pressure
W	Surcharge Loading Width
D	Surcharge Loading Distance away from the Shaft
θ	Dissipation Angle
E	Material Modulus of Elasticity
γ	Material Unit Weight
v	Material Poisson Ratio
c	Material Cohesion
τ	Shear Strength
σ	Principle Stress
s	Half of the difference between the maximum principal stress and the minimum principal stress
σ_1	Maximum Principle Stress
σ_3	Minimum Principle Stress
σ_m	Average Principle Stress
$q_{lateral}$	Lateral Earth Pressure
K	Coefficient of Lateral Earth Pressure
σ_2	Circumferential Stress
a	Shaft Outer Radius
b	Shaft Inner Radius
x	Distance from Shaft Center to a point on the wall
λ	The coefficient of tangential earth pressure

K_a	Coefficient of active earth pressure
δ	Wall friction angle
K_{wa}	Coefficient of earth pressure
β	The angle of slip surface
N_w	The lateral stress acting on the surface of wall element and is same as σ_h
σ'_v	Vertical stress at certain depth of z
A	The area of differential soil element
τ_f	The shear strength at failure surface
τ_w	The shear strength at wall surface
A_l	The horizontal area of loose zone
Pi	The total soil pressure

1. Introduction

1.1 General Retaining Systems

The structural elements that are designed to retain soil and rock slopes are called retaining systems. They connect two different earth elevations to hold on the lateral earth pressure. Various types of retaining systems are classified according to construction methodologies and applications. Ergun [1] provides a comprehensive review of various types of retaining systems such as braced walls, sheet walls, diaphragm walls and others. Figure 1 shows sample shoring systems [2] , [3].

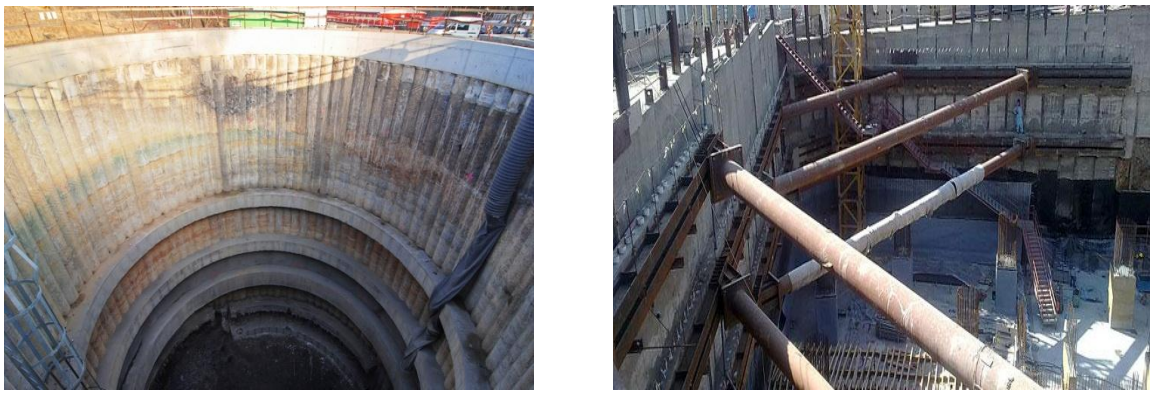

Figure 1. Examples of shoring system as presented in [2] and [3]

Braced walls are usually supported by struts, anchors, and/or nails, and are suitable for low cohesion soil. They are used for pipe lying, shallow tunnel installation and excavations with limited depth. Sheet walls are usually made of thin steel sheets with different prefabricated sections. Sheet walls can also be prepared using concrete. Steel sheets are preferred for use in stiff and dense soil, in which they are driven by hammers or vibrations, whereas concrete sheets are preferred for use in soft soil. Diaphragm retaining walls are formed by using various approaches such as slurry wall and secant pile wall techniques. These walls can be installed in different layouts depending on the shape of the required excavation and can be supported by various means as the excavation advances. Diaphragm walls are mostly used for deep excavations to provide soil support and waterproofing. Their thicknesses range from 0.5m to 1.5m and they are constructed in panels. The bentonite water mixer is used to prevent soil collapse in the excavation area before the steel cages are lowered and the concrete is poured.

Reinforced concrete retaining walls are another type of retaining system that are used for cohesive soil above the water level. These types of walls are supported by ground anchors. When holes are drilled into the supporting wall to insert reinforcing bars and grouting, the wall is called a soil nail wall. These wall segments are 1.5m – 2m high; shotcrete, wire mesh, and geotextiles are used in combination with a pattern of nails. Some retaining walls are used in the water rather than on land. For example, the cofferdams are temporary retaining systems which are used in marine environments, where they are expected to retain water to facilitate construction activities in coastal and sea environments. Apart from what has already been mentioned here, other retaining systems also exist, which include prefabricated diaphragm walls, jet grout and deep mixed walls, top down construction, and partial excavation or island method (see Ergun, 2008).

Retaining structures can also be classified according to their construction techniques and components instead of their functions. The most valuable retaining walls are those which consist of piles such as diaphragm walls, secant piles, and contiguous walls. Specifically, a secant pile wall is a special contiguous wall formed of overlapping primary and secondary piles. The construction process starts by lowering caissons while excavating inside; then the concrete is poured to form the individual piles, and multiple piles are constructed in an overlapping layout to form a continuous wall. The present study sheds light on the application of secant walls as retaining structures. The next section details the construction technique and the main advantages of using circular secant walls.

1.2 Secant Pile Walls

Secant pile walls are some of the most economical excavation water control systems that can be used in cofferdams, subway structures and tunnels as they can provide both vertical and horizontal support. These walls can be constructed in all patterns that form watertight walls or structural overlapping walls. Thus, secant pile walls can be used as structural foundations, retaining structures, and ground water barriers. They are easy to construct with good alignment precision, produce less noise relative to other shoring options, and can be constructed close to existing buildings. Moreover, secant pile walls in

a circular layout provide a unique advantage for access shafts since they behave as a compression ring under lateral earth and hydrostatic pressures as shown in Figure 2 [4].

Figure 2. Circular secant pile wall – Compression Ring

Secant pile walls consist of continuous intersected piles in which alternating piles are first constructed, leaving a required clear space in order to fit the intermediate piles, depending on how the piles are designed. Concrete with a slow rate of setting is poured after the excavation. Before the concrete sets, the intermediate pile cases with sharp edges are driven to cut the adjacent concrete in certain places. The procedure is repeated accordingly till the whole wall is completed. Secant pile walls can be built using various concrete compressive strengths with or without reinforcement depending on the type of application. Figure 3 shows secant piles during installation [5] and after construction [6].

Figure 3. Examples of (a) Secant pile forms, and (b) Secant piles with ties

The use of secant pile walls results in significant cost and schedule advantages. For example, the use of secant pile walls in a project executed by J Murphy & Sons in London to construct a pump station at Deepham Sewage Treatment Plant cut the

construction cost and schedule by £ 1.2M and 6 weeks (20% of the total cost & time) respectively [7].

1.3 Background and Literature Review

The scope of this study spreads into two main goals. The first is to enrich the background in the field of tunneling, and the second is to investigate the structural response of vertical access shafts for various soil-structure interaction (SSI) conditions. The most critical mechanisms of the circular shafts highlighted in this study increase understanding of their behavior. The following literature review is, therefore, conducted according to the main objectives of the thesis.

1.3.1 Studies on Lateral Earth Pressures

Determining the realistic values of soil pressures exerted on a circular shaft is essential for a successful design. The existing design methodologies for circular shafts in soil are based on a simple approach where the determination of soil pressures acting on the shaft wall and wall stability calculation are treated separately. Some of the existing theories include the plasticity equilibrium methods (PEM), such as the ones presented in [8] and [9], which are based on the equilibrium of yielded soil behind the support. Also, the limit equilibrium methods [10] assume a rupture surface. In comparison, the diaphragm walls installed to form a circular shaft are allowed to harden before the excavation proceeds, and thus it is assumed in the design practice that the in-situ stresses remain unchanged after the excavation (e.g., De Moor and Stevenson [11]). Accordingly, the earth pressures ranging from active to at-rest pressures are used in the design of such systems.

AlMadhoun [12] modeled the construction sequences as well as the time dependent medium of a circular shaft using a 2D Finite Element Analysis (FEA) approach. The simulation of the construction sequence indicated that stresses were much lower than those observed when the construction sequence was not considered in the FE modeling.

The effect of the earth pressures on a vertical circular shaft was investigated by various researchers using both centrifuge model tests and field tests. Kim et al. [13]

studied the effect of lateral earth pressures along the depth of a circular shaft using three dimensional (3D) FE models. It was found that the lateral earth pressures decreased as the relative displacement increased. Furthermore, comparing the results with those produced by the Rankine method showed that the latter approach overestimated the pressure values at certain depths by more than 80%. It was also shown that the stress arching effects were more pronounced at deep excavations compared to shallow excavations.

Tobar et al. [14] evaluated the earth pressures generated by granular soils on cylindrical shafts using various theoretical methods including the limit equilibrium and line slippage methods. These two methods were subsequently compared. Moreover, a simulation of radial soil movements, lining installation, shaft sinking, and temporary stabilization of the excavation using fluid pressure was performed. It was recommended to consider gravity by using full-shaft geometry and large-scale experiments. The theoretical approach provided very close results to the active earth pressure for the case of shallow excavation (i.e., at $H \leq 2r$ where H is the cylindrical shaft depth and r is the radius of the shaft). The results were, however, more sensitive to the ratio of horizontal to vertical arching affects at larger depths.

Liu [15] utilized the slip line method and FE modeling to study the axisymetric earth pressures acting on a circular retaining structure. The analysis took into consideration the arbitrary wall movement and the tangential stresses. It was assumed that both the internal soil friction and the wall friction develop with the wall movement. The results showed an exponential decrease of the lateral earth pressure with increasing wall movement. Finally, it was recommended to consider a large wall displacement of 0.3% of the height in practice.

Herten et al. [16] performed 3D calculations for spatial sand pressure on circular shafts using the PFC3D finite element program. The Distinct Element Method (DEM) was utilized and was verified with the analytical results. It was found that the DEM has the capability to model granular soils in static and dynamic states.

Ghanbari et al. [17] reviewed and proposed a formulation of the horizontal slices method to determine the effect of a line surcharge on a retaining wall. The proposed method indicated that an increase in the line surcharge increases the failure wedge angle, but the surcharge distance from the wall does not significantly affect the angle of the failure wedge. The results also showed increasing reinforcing forces along the wall height.

A new solution for the soil-wall system was developed by Caltabiano et al. [18] based on a pseudo-static equilibrium. This method considers the presence of the retaining wall and the surcharged backfill. The investigations were aimed at studying the seismic stability of the retaining walls, the effect of the surcharge intensity, and its distance from the wall. The proposed system was compared to another one that did not include surcharge. It was concluded that the soil-wall system with small surcharge intensity collapses when exposed to the smallest yield acceleration. For surcharged backfills at far distances, only surcharges with sufficient intensity affect the wedge failure mechanism.

Wang [19] used an analytical solution to calculate the lateral forces and their centroids on retaining walls. The investigations utilized an anisotropic backfill material in addition to different surcharge conditions, point loads, line loads, and rectangular area loads.

Yoo et al. [20] conducted a full scale test and 3D FEA to investigate the response of the geosynthetic reinforced wall, including two tiers, due to various surcharge loading levels. The results showed that the upper tier experienced higher horizontal stresses from the surcharge load than the lower tier. Also, the horizontal stresses decreased exponentially along the depth of the wall. The failure capacity was controlled by the backfill soil rather than by the reinforcement.

Hatami et al. [21] used a commercial FE software to simulate a full scale system consisting of four reinforced soil retaining walls that were influenced by a backfill compaction and different reinforcement types (polyester, welded wire mesh, and polypropylene). The predicted results were in good agreement with the measured values.

1.3.2 Studies on Shafts with Openings

The stresses generated in the shaft walls are calculated with the assumption of compression ring behavior, which results in purely compressive stresses. However, there are practical situations that will result in deviations from these stress conditions. For example, the excavation of a hole on the circular shaft yields a stress distribution in the shaft which will result in tensile stresses that are not observed in pure compression ring behavior. The theory that will be applied is subjected to the ratio of shaft radius to wall thickness.

Circular walls allow the applied pressure to generate hoop forces as internal reactions. The reactions are generated all around the circular wall in which only small shear forces and bending moments are developed, thus eliminating the need for external supports. The hoop stresses are resisted by the concrete strength through the wall thickness. Virollet et al. [22] indicated that the construction of a ring cannot be perfect because it is made of many panel sections, but the vertical tolerances shall be eliminated as much as possible. Also, buckling analysis should be considered for high compressive hoop stresses. An opening in the circular wall produces asymmetry and higher stresses around the opening which requires a 3D FE modeling for accurate analysis.

Makulsawatdom et al. [23] presented elastic stress concentration factors for internally pressurized, thick-walled cylindrical vessels with radial, offset circular, and elliptical cross holes.

Laczek et al. [24] performed an elasto-plastic analysis of stress-strain states in the vicinity of a hole in a thick-walled cylindrical pressure vessel using the finite element method.

Nihous et al. [25] studied elastic stress concentration factors for internally pressurized thick-walled cylinders with oblique circular holes using the finite element method and considering various wall ratios to cross-hole ratios.

Li et al. [26] employed inelastic FE analyses to study the effect of autofrettage on the stress levels in thick-walled cylinders with a radial cross-hole.

Duncan et al. [27] determined the effect of cross holes on the inelastic response by considering the shakedown and ratcheting behavior of plain thin and thick walled cylinders with radial cross-holes, subjected to constant internal pressure and cyclic thermal loading.

1.3.3 Studies on Rock-Socketed Shafts

Xiao-li et al. [28] proposed an analytical method based on the Hoek-Brown criterion to calculate the piles' embedment depth socketed inside a rock layer. The proposed method considered the rock properties in the analysis, and thus, compared well with other approaches such as the empirical method, elastic subgrade-reaction method and the MTC method for highway and port engineering.

Carter et al. [29] investigated the effect of lateral loads on the behavior of both rigid and flexible shafts socketed in rock by using the finite element method. The analysis included a parametric study for various material properties, loading conditions and relative stiffness with the incorporation of an overlying soil layer. The analysis results proposed a procedure to predict the lateral load capacity of the rock socketed shaft.

Various laterally loaded shafts socketed in rock were analyzed by Zhang et al. [30] by calculating the ultimate resistance of both the rock layer and the overlying soil layer. Nonlinear analysis was adopted to obtain the load-displacement response. The proposed method indicated good agreement with the field tests and the elastic solutions.

Lymon [31] utilized the p-y method and developed rational equations to analyze single piles in rock. The experimental results showed good agreement with the analytical method and verified the ability of the p-y method to analyze piles in rock rather than soil.

1.3.4 General Studies on Retaining Walls

Arai et al. [32] modeled the construction of the diaphragm wall and subsequent soil excavation using a three dimensional elaso-plastic finite element analysis. The wall was considered to be circular with 48 segments, with a 32m diameter, 1.2m thickness, 85.5m depth, and to pass three different soil layers which are clay, sand, and rock. The first panel was used to study the total horizontal stress distribution along the depth of the

gutter. Also, the effect of the initial panel construction on the total horizontal stresses for the same gutter was studied. The horizontal wall displacement along its depth was investigated due to the influence of wall thickness and initial panel construction. Moreover, the vertical displacements of the wall panel were monitored before and after the construction of the initial wall panel. The model was initially formulated as axisymmetric, but lost its uniform behavior once the initial stage of the construction was completed. The maximum lateral earth stresses after the excavation were found to be greater than the total initial horizontal stresses, whereas the minimum lateral earth stresses after the excavation were less than the total initial horizontal stresses.

Thasnanipan et al. [33] studied the diaphragm wall construction practices in Bangkok and suggested the use of a top-down construction method, and ground improvement to enhance the water prevention system of the diaphragm construction.

Guler [34] proposed an approach to determine the lining thickness of the support shafts by estimating the pressure distribution on the shaft via a 2D numerical simulation considering different rock strengths and in situ non-hydrostatic stresses.

Guichard et al. [35] studied the vertical access shafts for Mexico tunnels constructed in soft clays. Different construction stability states were investigated to ensure the serviceability of the shaft. Guide wall stability and nucleus stability were assessed using the finite element method. Also, excavation stability, bottom uplift failure, floating, long-term behavior, and movements of neighboring buildings were investigated. The soil fracture was monitored, and it was concluded that soil fracture could happen when the slurry level is around 1m above the water table. The researchers showed that the slurry level is very critical for safety. The safety of the shafts decreased with an increase in shaft diameter. The researchers also reported that the axisymetric finite element method was very useful in assessing the safety of the access shaft.

Sanada et al. [36] conducted mine-by experiments to examine the development of the excavation damaged zone in a deep shaft that was constructed in sedimentary rock. Boreholes were excavated at different distances from the shaft, and the mechanical properties were studied by performing borehole television, permeability tests, expansion

tests, and seismic velocity tests. Breakout was observed within 1m of the shaft while it was not observed in the boreholes that were placed 8m away from the shaft. Furthermore, the hydraulic conductivity increased in the close boreholes but did not change in the far boreholes. The seismic velocities showed that no changes were observed before and after the shaft sinking. The elastic moduli decreased after the shaft sinking while large compressive strains were monitored at 0 to 100 cm from the borehole collars. A two-dimensional numerical analysis was also conducted to interpret the in-situ results.

Yansen et al. [37] investigated the effect of additional vertical stresses on a shaft wall caused by a drainage aquifer layer. Numerical studies were carried out to investigate the stress effect on the wall. It was concluded that the prediction of a vertical stress increase was not certain because of the difficulty in understanding the wall-medium interaction. Also, the design principle of "resist" was over conservative for the wall structural design; however, the "resist and yield" design principle produced an economical and safe wall structural design.

A 3D Finite Element Analysis was performed by Bryson et al. [38] to inspect the ground movement due to the adjacent structures. In this study, secant pile retaining walls were installed on the sides of the Chicago and State Street subway tunnel station. The model analyses proved that the adjacent structures increase lateral deformation. Also, the stress relief caused higher shear stresses in the soil. The observed data, not the model, showed that the existence of a school on one side of the tunnel had reduced lateral deformation due to the stiffness added to the soil. It was suggested to add the wall construction technique to the model in order to enhance the accuracy of the results.

Yeh et al. [39] studied the dynamic response of the circular shaft under torsion effects using both the analytical solution and the experimental method. A good agreement between the results of experimental and analytical methods was reached.

Liang et al. [40] used 3D Finite Element modeling to study the mechanism of slope arching with equally spaced drilled shafts socketed in a rock layer. The parametric study included the rigidity of the shafts, the socketed length, the shafts' spacing and locations, and soil movements and strength parameters. Regression analysis was then performed to

obtain the load transfer factors from the soil slope arching. The results showed that the parameters that affected the load factor the most were the drilled shaft properties, the rock modulus, slip surface depth and soil cohesion, friction angle and field displacement. The slope's factor of safety could be improved significantly by ensuring that the shafts are drilled sufficiently into the rock layer or by spacing them at distances equal to four times the shaft diameter.

Laterally loaded rigid piles in cohesionless soil were studied by Zhang [41] using non-linear analysis. The response of the piles was calculated assuming a linear increase of both the soil resistance and the lateral subgrade modulus with depth. The analysis results were verified by comparing them with those of Finite Element Analysis and the centrifuge test.

The soil arching phenomenon makes the distribution of lateral earth pressure rounded rather than horizontal. Handy [42] concluded that soil arching reduces the pressure distribution compared to Coulomb analysis. However, the soil action shifted the center of soil pressure to a higher elevation compared to other analyses.

Theoretical and numerical analyses were carried out by Yamamoto et al. [43] to investigate the effect of surcharge loading on the stability of square tunnels in cohesive-frictional soils based on the plain strain assumption. It was indicated that the shallow circular tunnels have higher ultimate surcharge loading compared to the shallow square tunnels.

Iskander et al. [44] used built-in defected drilled shafts to examine the ability of nondestructive tests (NDT) to detect shaft defects and their effect on shaft capacity. The investigated defects were soil inclusions, soft bottom and voids. The defects that had a size larger than 10% of the cross section were detected easily. Results also showed that the soft bottom condition decreased the end bearing capacity by 33% while reloading reduced the strength by 20% and the skin friction by 30%.

Kruse et al. [45] analyzed a large diameter shaft subjected to seismic loading using 2D and 3D finite element models. The shaft was constructed using a top-down method in which precast concrete segments, ring assembly, ring beams, and starter rings were used.

It was designed as a temporary retaining structure with a permanent vertical support system. The analysis indicated that ring stability was affected by the soil-structure interaction, but it was not affected by the soil stiffness/strength and soil loading patterns. Moreover, the ring beam and the post shores increased the ring critical buckling while the starter ring decreased the deformations.

In summary, a review of the literature sources reveals valuable and sufficient information for understanding the behavior of retaining walls under various circumstances. The background includes different procedures to calculate the lateral earth pressure on either circular or straight retaining walls. The available procedures include analytical approaches such as the Limit Equilibrium, the Distinct Element, and the Line Slippage methods; in addition there are field tests, centrifuge models, and Finite Element Methods. Also, the literature presents different approaches for calculating the magnitude and location of surcharge pressure on retaining walls. The analyses again include the application of full scale tests, 3D Finite Element Analysis, seismic stability tests, and the horizontal slices method. Design solutions for shafts socketed in rock layers are also provided. However, the literature lacks studies on circular diaphragm walls that are constructed using secant pile systems. Because these walls have special mechanisms, it is important to study their behavior for different applications. Moreover, since the literature shows the strength of 3D Finite Element modeling for very complicated geotechnical problems, nonlinear finite element analysis is utilized in this study using the commercial finite element package, ABAQUS [46].

The present study enhances the research background on the design aspects of circular secant pile walls. The analysis will cover the behavior of circular shafts subjected to different exposures. The findings will be used as design guidelines for circular shafts inserted in cohesionless soil, subjected to unbalanced loadings, socketed in inclined rock layers, and used for tunneling purposes.

1.4 Objectives & Methodology

1.4.1 Project Objectives

This thesis investigates the structural response of vertical shafts considering Soil-Structure Interaction with various soil conditions. The main objective of this study is to develop a comprehensive approach to the design of vertical shafts. It is expected to provide solutions to the mechanics of circular shafts.

The following steps provide additional details about the objectives:

1- To develop a 3D nonlinear finite element (FE) model capable of simulating the structural response of a circular shaft inserted in soil. The FE model will be verified by comparing displacements, vertical pressure distribution, and circumferential stresses with existing analytical solutions and field data.

2- To investigate the effect of different shaft parameters such as the depth, diameter and thickness on the mechanics and overall response of the circular shaft system.

3- To study the structural response of circular shafts that consist of one or two holes. The main purpose is to investigate the effect of stress concentrations encountered around the holes.

4- To study the mechanics of a circular shaft and its base stability when subjected to unbalanced earth pressures such as those from construction equipment.

5- To investigate the stress of embedded circular shafts in an inclined rock layer.

1.4.2 Methodology

As stated earlier, the circular shafts will be studied numerically using Finite Element Methods with the consideration of Soil-Structure-Interaction. The FE modeling will be conducted using the commercial software, ABAQUS [46]. The results predicted by the FE analysis will be validated using monitoring data of an existing vertical shaft construction, and also will be compared with analytical solutions. The RWH Engineering (a deep foundation construction company in Ontario, Canada), which carried out the design and construction of many vertical shafts, provided monitoring data for verification. The data is for a construction project of a vertical shaft that was installed in Waterloo, Canada. The RWH team installed two inclinometers on the caisson wall

circular shaft to monitor the displacements in the major axes. The monitored data obtained during the construction was provided. The verified FE model will then be used to conduct a parametric study investigating various design aspects for vertical shafts. The circular shafts will be investigated considering various soil conditions. The homogenous soil stratigraphies including cohesionless soils will be considered. An elasto-plastic constitutive relation will be used to model the soil behavior. On the other hand, the concrete material used for the shaft will be assumed as linear elastic. Details about the parametric study are outlined below.

1. Compression ring:

The behavior of a compression ring in cohesionless soil is affected by several parameters that are summarized in Table 1.

Table 1. Compression Ring Parameters and Values

Radius (m)	Soil friction angle (Ø)	Depth - H (m)
3	30°	3, 6, 9, 12, 15, 18, 21, 24
	35°	3, 6, 9, 12, 15, 18, 21, 24
	40°	3, 6, 9, 12, 15, 18, 21, 24
5	30°	5, 10, 15, 20, 25, 30, 35, 40
	35°	5, 10, 15, 20, 25, 30, 35, 40
	40°	5, 10, 15, 20, 25, 30, 35, 40
10	30°	10, 20, 30, 40
	35°	10, 20, 30, 40
	40°	10, 20, 30, 40

2. Existence of one and two holes in a shaft:

Tables 2 and 3 detail the examined parameters in this study. Also, the parameters are explained clearly in Figure 4.

Table 2. Parametric study of a shaft with ONE hole

Shaft Radius (m)	Hole radius (m)
5	0.5, 1, 1.5, 2
10	1, 1.5, 2, 3, 4
15	1.5, 2, 3
20	1.5, 2, 4

Table 3. Parametric study of a shaft with TWO holes

Shaft Radius (m)	Hole radius (m)	Distance between holes ($x.r$)
5	0.5	2, 4
	1	2, 6, 10, 14
	1.5	2, 6
	2	2, 6
10	1.5	2, 6, 14
	2	2, 4, 6
	3	2, 6
	4	2, 4

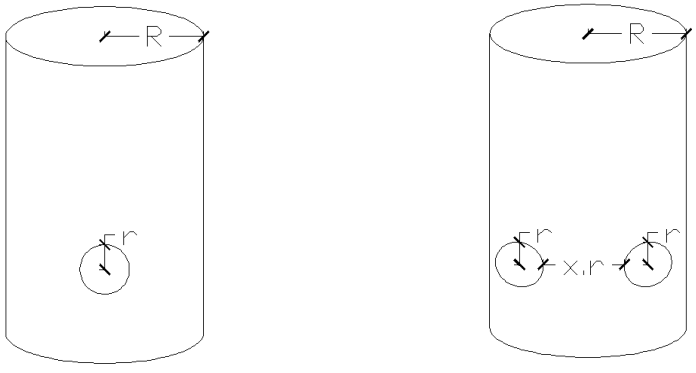

a **b**

Figure 4. Shaft with (a) One hole opening, and (b) Two hole openings

3. Rock-socketed shaft:

The studied parameters of the rock layer are summarized in Table 4.

Table 4. Rock Socketed Shaft parametric study

	Case 1	Case 2	Case 3	Case 4
Angle	0°	10°	20°	30°
Shaft socketing distance	2.5 m	2.5 m	2.5 m	2.5 m
Maximum shaft height	25 m	25 m	25 m	25 m

4. Loading Conditions:

The loading effect includes the load magnitude, width, and distance for different shaft geometries and soil properties. The parametric study is summarized in Table 5 and the parameters are shown in 3D configuration in Figure 5.

Table 5. Unbalanced loading parametric study

Radius (m)	Soil friction angle (Ø)	Distance from shaft edge (m)	Loading Width
3 & 5	40º 30º	0	3
			6
			12
			24
			40
			48
		3	3
			6
			12
			24
			40
			48
		6	3
			6
			12
			24
			40
			48

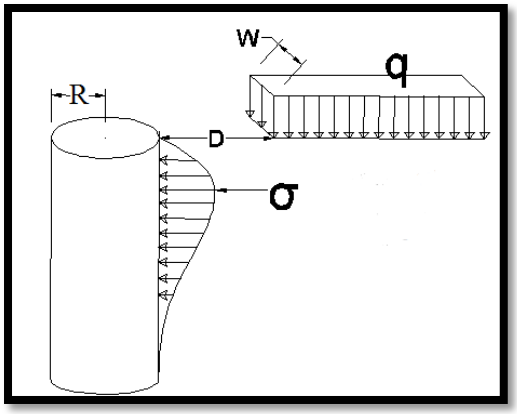

Figure 5. Surcharge loading parameters

5. Soil & Rock material properties:

The investigated Granular soils with various strength and stiffness values are listed in a later section in Table 6 while Tables 7 & 8 summarize the concrete and rock material properties, consequently.

2. Theoretical Background

Analytical and numerical studies have shown that the pressures acting on the exterior surfaces of a circular shaft are less than at-rest pressures assumed in plane strain conditions due to the stress relief during the excavation, if sufficient deformations occur in the wall (Shin and Sagong [47]). Horizontal arching effects also influence the distribution of earth pressures on the circular exterior surface of the walls. However, due to the construction techniques employed in the construction of secant pile walls, only small deformations take place and the deviation of earth pressures form at rest conditions towards active conditions is very low since the wall deformations remain insignificant even at large shaft diameters. The stresses generated in the shaft walls are calculated with the assumption of compression ring behavior, which results in purely compressive stresses.

Determining realistic values of soil pressures exerted on the circular shaft is essential for a successful design. The existing design methodologies for circular shafts installed within soil are based on an approach where the determination of soil pressures acting on the shaft wall and wall stability calculation are treated separately. The plasticity equilibrium methods (PEM) such as those used by Terzaghi [8] and Berezantzev [9] are based on the equilibrium of yielded, plastic soil behind the shaft walls. Limit equilibrium methods such as Prater [10] assume a rupture surface. The convergence confinement method (CCM) takes into account the design parameters such as in situ stress field, ground and support properties, and construction sequence, and allows prediction of the soil deformation and formation pressure simultaneously (Wong and Kaiser [48]). Houlsby and Wroth [49] have determined the lateral earth pressures for a smooth axisymetric wall by the method of characteristics. This method assumes level ground and considers both cohesive and cohesionless soil conditions. Drescher [50], [51] provided a detailed treatment of the stability of a vertical circular shaft cut by the method of characteristics for level ground. Jenike and Yen [52] have proposed solutions for the ultimate active pressure for “rat-holes” which are later extended by Hill and Cox [53]. The solutions to the rat-hole by Jenike and Yen [52] or Hill and Cox [53] represent only

the ultimate condition which is stabilized at a relatively great depth; the pressure distribution at the top of the circular shaft is not determined.

Due to the unique approach used in their construction, the treatment of the earth pressures on diaphragm walls differ from the situations where the above-mentioned solutions described above are applicable. The diaphragm walls installed to form a circular shaft are allowed to harden before the excavation proceeds, and thus it is assumed in design practice that in-situ stresses in the ground remain unchanged after the excavation (e.g., De Moor and Stevenson [11]). There are studies which suggest that the earth pressures behind diaphragm walls are affected by the installation. Among them are Arai et al. [54], Gunn et al. [55], Gunn and Clayton [56], Kutmen [57], De Moor [58], and Ng and Yan [59] who studied the installation effect considering plane strain conditions. The installation effects for the circular shafts were studied by many researchers including but not limited to Goto et al. [60], Ariizumi et al. [61], Muramatsu and Abe [62], and Arai et al. [54]. A number of reduced scale model tests investigating the interaction between the circular shaft and surrounding soil exist in the literature. For instance, Muller-Kirchenbauer et al. [63] studied the earth pressures exerted on a circular shaft by dry sand. The results of this study indicated that the ultimate pressures correspond to the rigid models that do not allow recess. However, the more flexible models that allowed wall deformations exhibited a larger reduction in pressures. Lade et al. [64] studied the earth pressures exerted on a vertical circular shaft in dry sand using centrifuge testing. The results of these tests showed that the earth pressures slightly exceeded at-rest values prior to the excavation of the soil inside the shaft. However, with the excavation of the soil and resultant inward movement of the shaft walls, earth pressures reduced substantially. Shin and Sagong [47] performed model tests to determine the earth pressures on a circular shaft. Their results indicated that the earth pressures on the shaft decrease substantially if there are wall deformations larger than 1.5% of the shaft radius. At small deformations, the earth pressures remained between at-rest and active conditions.

2.1 Earth pressures

The vertical shaft behavior is significantly influenced by the gravitational forces and resultant stress state in the surrounding soil (Wong and Kaiser [48]). Kim et al. [65]

provides a comprehensive summary of the earth pressure assumptions typically used in practice. Due to the 3-dimensional nature of the stress concentrations near a vertical circular shaft, a difference between vertical and radial stress components around the shaft occurs (Figure 6a). A common shape assumption for a failure wedge is depicted in Figure 6b, where $\beta = 45° + \emptyset/2$. A summary of tangential and radial earth pressure assumptions outlined in Kim et al. [65] is presented in Figure 6.

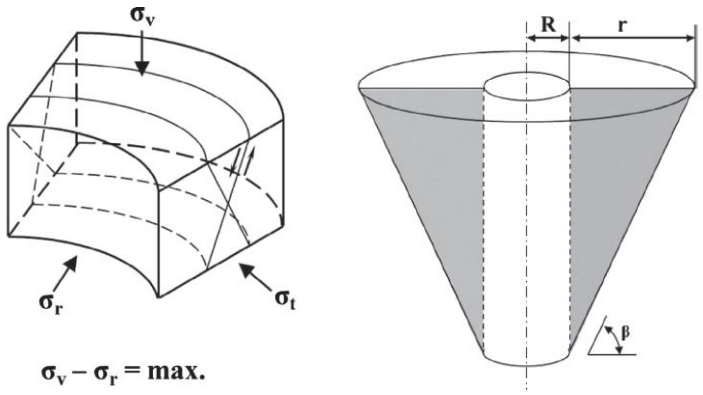

Figure 6. Behavior of the soil around vertical circular shaft: (a) Mode of yielding and (b) Slip surface.

The coefficient of tangential earth pressure (λ) is defined to be the ratio of tangential stress to vertical stress. The earth pressures on vertical shafts decrease with the increase of tangential stress acting on the failure surface with the increase of (λ) value. Wong and Kaiser [48] suggested that (λ) value is not 1.0 at elastic state; but will reach 1.0 at plastic state. Lee et al. [66] suggested a relationship between λ and the friction angle $\emptyset$ as follows: $\lambda = 1 - \mathrm{Sin}(\emptyset)$. Rankine [67] suggested the coefficient of active earth pressure (K_a) without considering the wall friction angle (δ). Paik and Salgado [68] assumed minor principle stress direction was changing in a concave shape, such as elliptic, catenary and parabolic, due to the level fictional resistances of the wall, and the coefficient of earth pressure (K_{wa}) which was given as follows:

$$K_{wa} = \frac{3(N.\cos^2(\theta)+\sin^2(\theta))}{3N-(N-1)\cos^2(\theta)} \quad (1)$$

where, $N = \tan^2(45° + \emptyset/2)$, $\emptyset = \tan^{-1}\left[\frac{\left(N-1\pm\sqrt{(N-1)^2 4N\tan^2(\delta)}\right)}{2\tan(\delta)}\right]$ and δ is the wall friction angle in degrees. The equilibrium condition of horizontal force acting on the differential soil element results in the following (see Figure 7):

$$\int_0^{2\pi} N_w R d\theta dz + \int_0^{2\pi} 2\sigma'_t \sin\left(\frac{d\theta}{2}\right) r dz + \int_0^{2\pi} \tau_f \left(\frac{\cos\beta}{\sin\beta}\right)(r+R) d\theta dz = \int_0^{2\pi} N_f \left(\frac{\cos(90°-\beta}{\sin\beta}\right)(r+R) d\theta dz \quad (2)$$

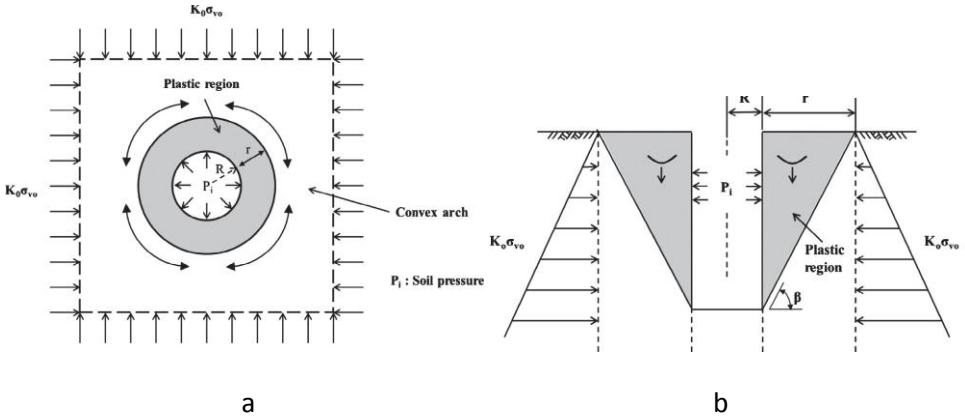

Figure 7. (a) Lateral arching pressure (b) Vertical arching pressure (after Kim et al. [69]**)**

In Eq. [2], N_w is the lateral stress acting on the surface of the wall element and is same as σ_h, and τ_f is defined as shear strength at the failure surface. N_w and σ'_t can be expressed as follows:

$$N_w = \sigma'_h = \mathrm{K_{wa}} * \sigma'_v \quad (3)$$

$$\sigma'_t = (1 - \sin\emptyset) * \sigma'_v \quad (4)$$

where, σ'_v is the vertical stress at a certain depth of z. If $d\theta$ is very small, substitution of Eq. [3] and [4] into [2] leads to the expression shown in Eq. [5].

$$N_f = \frac{RK_{wa}\sigma'_v + r(1-\sin\emptyset)\sigma'_v + c\frac{\cos\beta}{\sin\beta}(r+R)}{(r+R)} - \frac{\tan\beta}{\tan\beta - \tan\emptyset} \quad (5)$$

From Figure 8, the equilibrium of vertical stress gives

$$\sigma'_v A + Adz\gamma = (\sigma'_v + d\sigma_v)A + 2\pi R\tau_w dz + 2\pi R\tau_w dz\{\tau_f sin\beta + N_f \sin(90-\beta)\}\frac{dz}{sin\beta} \quad (6)$$

where A is the area of the differential soil element, τ_f is the shear strength at the failure surface, and τ_w is the shear strength at the wall surface. By substituting Eq. [5] into Eq. [6], the first order differential equations depicted in Eq. [7] can be obtained.

$$\frac{\partial \sigma'_v}{\partial z} + S\sigma'_v = T \tag{7}$$

for $z = 0$, $\sigma'_v = 0$, thus

$$\sigma'_v = \left(q - \frac{T}{S}\right) e^{-Sxz} + \frac{T}{S} \tag{8}$$

Parameters T and S can be expressed as

$$T = \gamma - \frac{2\pi}{A_l}\left\{c_w + c(R+r)\left(1 + \frac{1}{tan\beta} + \frac{1+tan\beta * tan\emptyset}{tan\beta - tan\emptyset}\right)\right\} \tag{9}$$

$$S = \frac{2\pi}{A_l}\left\{k_{wa} + Rtan\delta + (k_{wa}R + \lambda r) + \left(\frac{1+tan\beta * tan\emptyset}{tan\beta - tan\emptyset}\right)\right\} \tag{10}$$

where γ is the unit weight of the soil (kN/m^3), ϕ is the soil friction angle (°), c is the soil cohesion (kPa), R is the radius of the shaft (m), r is the radius of the plastic region in a definite depth (m), A_l is the horizontal area of the loose zone (m^2), β is the angle of the slip surface, and q is the surcharge load. Thus, the total soil pressure (Pi) can be given as

$$P_i = \mathrm{K_{wa}}\sigma'_v \tag{11}$$

where $\mathrm{K_{wa}}$ is the coefficient of radial earth pressure, and σ'_v is the effective vertical overburden pressure.

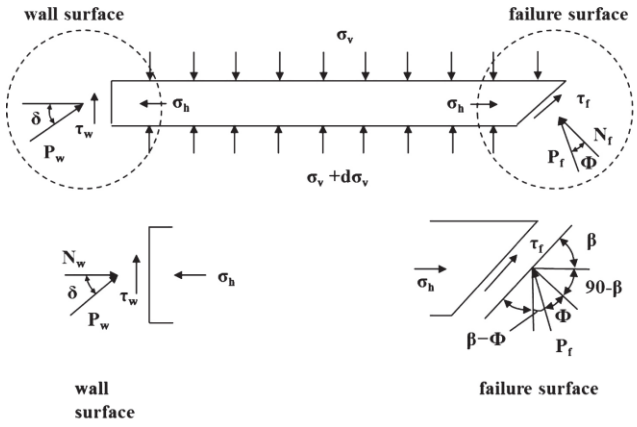

a

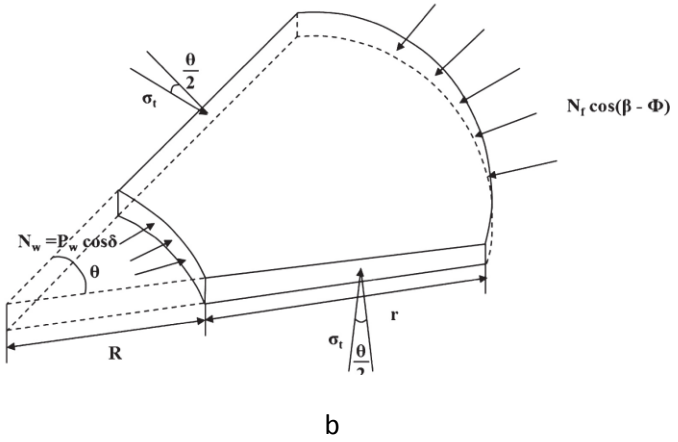

Figure 8. (a) Lateral arching pressure (b) Vertical arching pressure (after Kim et al. [69]**)**

2.2 Wall stresses

The design of circular diaphragm walls is typically performed using closed form analytical solutions assuming a uniform external pressure distribution to represent the earth pressures, hydrostatic pressures and surcharge. The steps that are followed include the estimation of external pressures (earth + hydrostatic + surcharge) on the exterior of the circular secant pile wall, as well as calculation of the stresses and subsequent deformations in the wall under assumed external pressures. The validity of the external pressure assumptions can be re-evaluated using monitoring results of shaft movements.

Stresses in circular diaphragm walls can be estimated by determining the distribution of stresses in a cylinder subjected to uniform radial pressures, which change with depth, acting on the outer surface of the shaft. The theory that will be applied is tested by investigating the ratio of shaft radius to wall thickness. However, the parametric analyses and the case studies presented in this study comprise walls that fall under the thick-walled cylinder category, and thus the relevant theory was implemented.

If the wall thickness of a cylinder is more than $1/10^{th}$ of the radius, the meridional and hoop stresses cannot be considered uniform throughout the thickness of the wall and the radial stress cannot be considered negligible. These wall stresses in thick cylinders must be taken into account (see Figure 9). For a thick-walled cylinder, which is subjected

to a uniform external radial pressure q and longitudinal pressure of zero (or externally balanced), the stresses and changes in cylinder dimensions can be expressed as

$$\sigma_1 = 0 \tag{12}$$

$$\sigma_2 = \frac{-qa^2(b^2+x^2)}{x^2(a^2-b^2)},\ (\sigma_2)_{max} = \frac{-q2a^2}{(a^2-b^2)} \qquad \text{at } x = b \tag{13}$$

$$\sigma_3 = \frac{-qa^2(x^2-b^2)}{x^2(a^2-b^2)},\ (\sigma_3)_{max} = -q \ \text{ at } \qquad x = a \tag{14}$$

$$\tau_{max} = \frac{(\sigma_2)_{max}}{2} = \frac{qa^2}{(a^2-b^2)}, \ \text{ at } \ x = b \tag{15}$$

$$\Delta_a = \frac{-qa}{E}\left(\frac{a^2+b^2}{a^2-b^2} - \mu\right),\ \Delta_b = \frac{-q}{E}\left(\frac{2a^2}{a^2-b^2}\right),\ \ \Delta_L = \frac{-q\mu l}{E}\left(\frac{2a^2}{a^2-b^2}\right) \tag{16}$$

where σ_1, σ_2 and σ_3 are stresses in the longitudinal, circumferential and radial directions, respectively (see Figure 9). Likewise, Δa, Δb and ΔL are the changes in the dimensions of a, b and L, respectively. The major parameters to be considered for an analytical design for diaphragm wall circular shafts are the values of the maximum external radial pressure q, the stresses in the wall section, and the change in the radius.

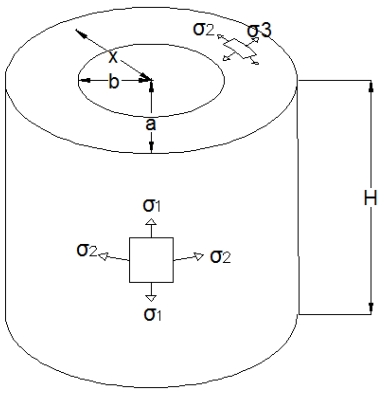

Figure 9. Cylindrical disk or shell

2.3 Thick-walled cylinders with holes

Some literature exists on the behavior of thick-walled cylinders with holes. For example, Makulsawatudum et al. [23] presented elastic stress concentration factors for internally pressurized thick walled cylindrical vessels with radial, offset circular and

elliptical cross holes. Laczek et al. [24] performed an elasto-plastic analysis of stress-strain state in the vicinity of a hole in a thick walled cylindrical pressure vessel using finite element method. Nihous et al. [25] studied elastic stress concentration factors for internally pressurized thick-walled cylinders with oblique circular to cross holes using finite element method considering various wall to cross-hole ratios. Li et al. [26] employed inelastic FE analyses to study the effect of auto frottage on the stress levels in thick-walled cylinders with a radial cross-hole. Duncan et al. [27] determined the effect of cross holes on the inelastic response by considering the shakedown and ratcheting behavior of plain thin and thick walled cylinders with radial cross-holes, subjected to constant internal pressure and cyclic thermal loading. No literature was encountered on the stress regimes around a hole in a large diameter thick-walled cylinder such as the secant pile wall circular shaft. Factors such as the external pressure distributions around a circular shaft and the location of the hole along the height of the shaft are the factors complicating the stress regime around the hole making an independent evaluation necessary.

The stress concentration factors determined using finite element analyses were compared with those obtained using the circular hole in an infinite plate solution (Roark et al. [70]). Figure 10 depicts the stresses on the plate. The maximum stresses under uniaxial conditions, where $\sigma_2=0$, were $3\sigma_1$ and σ_1 at the maximum compression and tension points, A and B respectively.

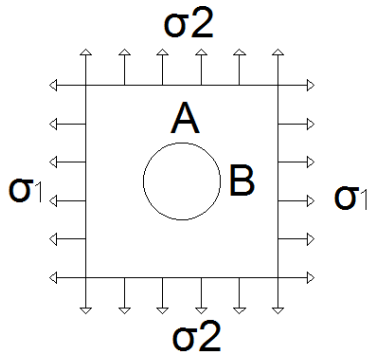

Figure 10. Elastic stress, in-plane normal stress

3. Finite Element Modeling

3.1 Geometric description

Each analysis step of this study requires a different model geometry for either the soil or the concrete shaft depending on the results sought. The basic geometry of soil is a block which contains a circular hole that extends according to the shaft's basic geometry for a specific height and thickness (see Figure 11). Therefore, a solid part definition was utilized for the soil geometry, whereas a shell part definition was adopted for the circular shaft.

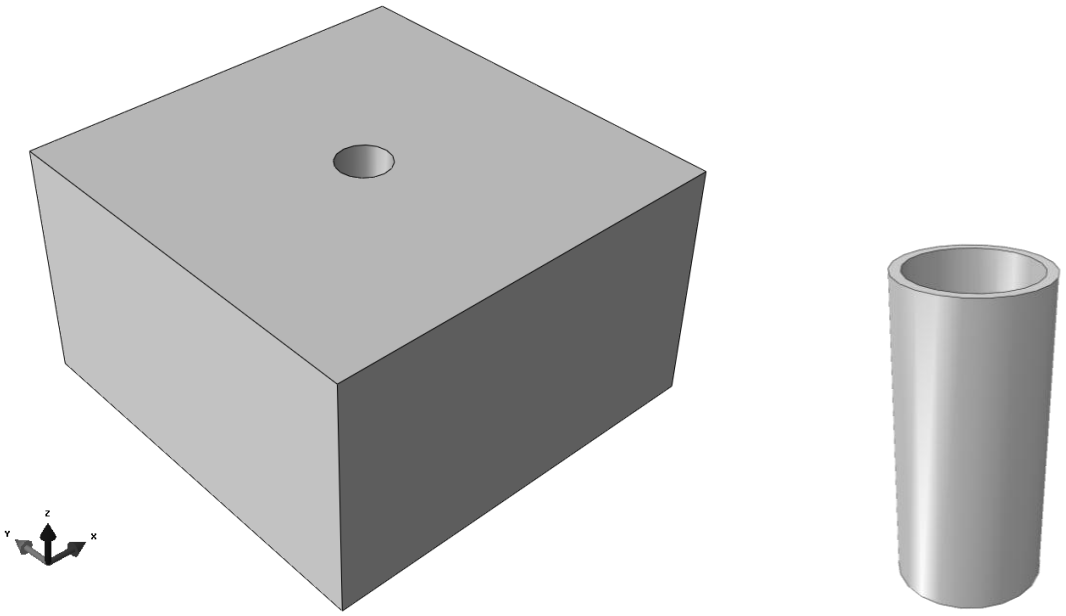

a **b**

Figure 11. (a) Basic soil block, and (b) Basic circular shaft

The soil dimensions depend on the shaft radius and depth. Soil length and width are almost equal, ranging from 30m × 30m to 200m × 200m, while the depths extend enough below the shaft to eliminate the boundary effect. Shaft radii range from 5m to 20m with a constant wall thickness. Figures 12 and 13 illustrate the soil geometries that are required for investigating the surcharge effect and the existence of inclined rock layers interfering with the concrete shaft.

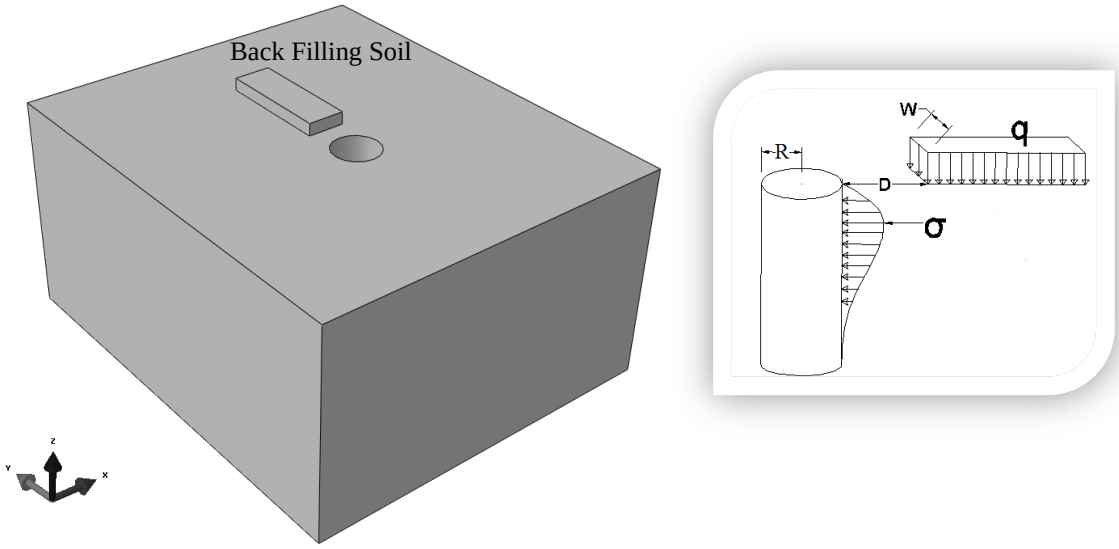

a **b**

Figure 12. (a) Soil model with back filling block, and (b) Layout of the surcharge loading

Various parameters are implemented in the surcharge loading model such as the surcharge magnitude (q), distance between the shaft and the backfill (D), width of the backfill, and the size of the shaft that is exposed to such loading.

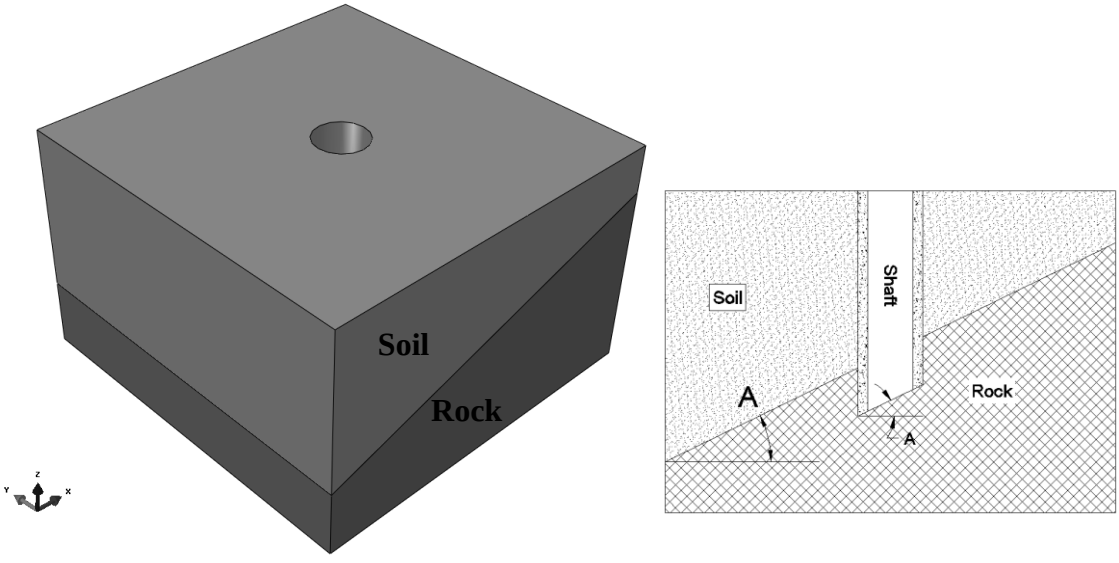

a **b**

Figure 13. (a) Soil layer overlying inclined rock layer, and (b) Cross section at the middle of the block

Figure 13(b) shows the inclination angle (A) of the rock layer and the shaft that is inclined by the same angle. The angle (A) has values of 10°, 20° and 30° and the socketed shaft distance in the rock is limited to 2.5m.

Figure 14(b) shows a shaft with a circular hole opening of diameters ranging between 1.0m and 8.0m, and for different shaft radii, 5m, 10m, 15m, and 20m. A two-hole shaft example is presented in Figure 14(c), where the distance between the adjacent holes of radius (r) is a function of the hole radius, 2r – 14r. This study covers two hole diameters, 1m and 2m, for two shaft diameters of 5m and 10m.

a **b** **c**

Figure 14. (a) Circular shaft socketed in an inclined rock layer (b) Circular shaft with One circular hole (c) Circular shaft with Two circular holes

3.2 Material Properties

The soil stratigraphy comprised a single uniform layer of cohesionless soil with isotropic properties. An elasto-plastic model with the Mohr-Coulomb failure criterion was utilized to represent the behavior of soil while a linear elastic behavior was assumed for the concrete material that was used to model a secant pile wall. The material properties of the soil, rock and concrete used in the present FE simulations are summarized in Tables 6, 7, and 8, respectively. The ground water table was assumed to be deep and its influence on the interaction between the secant pile wall and the surrounding soil was neglected for the sake of simplicity.

Table 6. Soil material properties

Friction angle $\emptyset$	Modulus of Elasticity E (Mpa)	Unit weight γ (kg/m^3)	Poisson ratio v	$Cohesion$ c
Soil 1 (40^0)	50	1900	0.25	0
Soil 2 (35^0)	30	1800	0.3	0
Soil 3 (30^0)	10	1700	0.35	0

Table 7. Concrete shaft material properties

Modulus of Elasticity E (Mpa)	Unit weight γ (kg/m^3)	Poisson ratio v
15000	2300	0.25

Table 8. Rock material properties

Friction angle $\emptyset$	Modulus of Elasticity E (Mpa)	Unit weight γ (kg/m^3)	Poisson ratio v	$Cohesion$ c (Mpa)
35^0	200	2500	0.3	0.2

3.2.1 Mohr-Coulomb Plasticity Model

The elasto-plastic behavior of the cohessionless soil considered in this study was modeled using the Mohr-Coulomb failure criterion which illustrates the failure conditions of an isotropic material [71]. The experiments show that the criterion is appropriate when principle stresses are all compressive while some modifications are needed for the tensile principle stresses [72]. Coulomb assumed a linear failure relation between shear stress (τ) and compressive stress (σ) [73], while Mohr assumed that the failure is only related to minimum principle stress (σ_1) and maximum principle stress (σ_3) [74]. The Mohr-Coulomb failure criterion is already implemented in the ABAQUS formulation. The plastic behavior can be modeled using either the Mohr-Coulomb surface or the Rankine surface for the tension cutoff (for more details see ABAQUS Documentation [75]). Figure 15 shows Mohr's circles, where the best line that touches the circles is the yielding line of the material. The failure criterion is related linearly to the principle stresses.

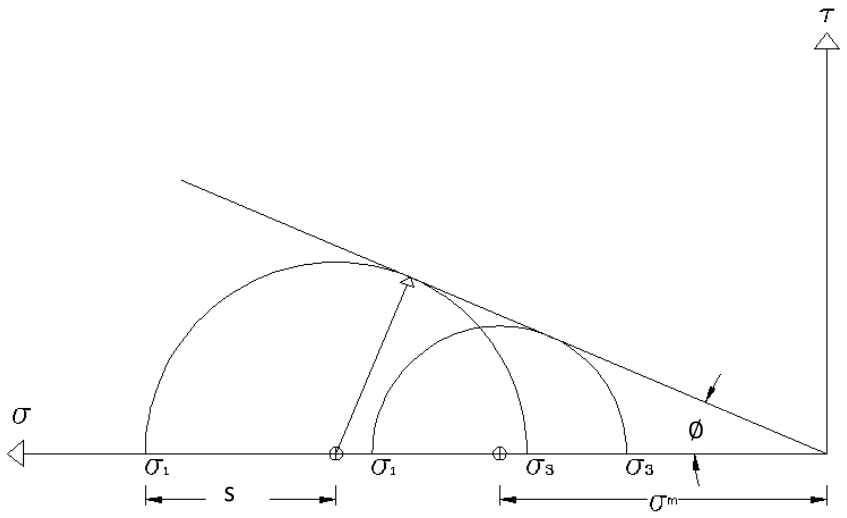

Figure 15. Mohr's circle

Therefore, the Mohr-Coulomb model is defined by

$$\tau = c + \sigma.tan\emptyset \quad (17)$$

where $\emptyset$ is the friction angle and c is the material cohesion. From Mohr's circle,

$$\tau = s.cos\emptyset \quad (18)$$

$$\sigma = \sigma_m + s.sin\emptyset \quad (19)$$

Substituting for τ and σ, and multiplying both sides by $sin\emptyset$, the Mohr-Coulomb model can be rewritten as follows:

$$s + \sigma_m sin\emptyset - c\,cos\emptyset = 0 \quad (20)$$

where $s = \frac{\sigma_1 - \sigma_3}{2}$ is the maximum shear stress, $\sigma_m = \frac{\sigma_1 + \sigma_3}{2}$ is the corresponding normal stress, and σ_1 and σ_3 denote the maximum and minimum principal stresses, respectively. For more details, see ABAQUS Documentation [75].

3.3 Boundary Conditions & Contacts

The realistic Soil-Shaft behavior is modeled by considering an initial geostatic step to define the gravity loading and also to establish an initial stress regime in the ground. The boundaries in each model were assumed to be at least five times the shaft depth (H) from the edge of the circular shaft to ensure that vertical boundaries do not affect the stresses in and around the shaft. A soil depth of at least one shaft depth (H) was maintained below the bottom of the shaft in all models. Displacement boundary conditions at the side

boundaries were fixed in both horizontal directions (x-axis & y-axis) and set free in vertical direction (z-axis), while they were fixed in both horizontal and vertical directions at the model base, Figure 16.

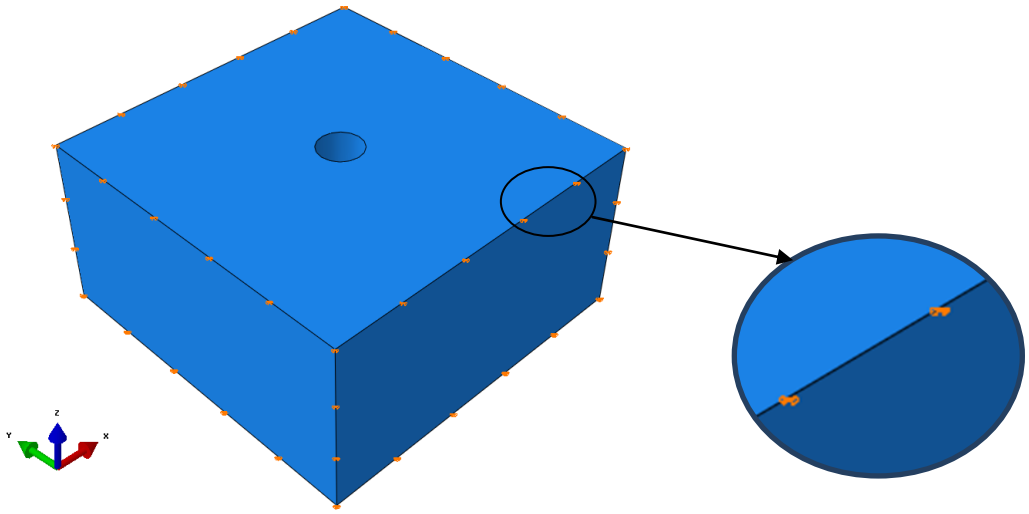

Figure 16. Boundaries of the Soil Model

The contact condition between the different parts needs to be well-defined to represent the real behavior of the Soil-Structure-Interaction (SSI). The concrete shaft has two main types of contacts with the surrounding soil. First, the shaft is assumed to have a tie constraint at the bottom edge with the soil. Second, normal and tangential surface-to-surface contacts with an allowed finite sliding are defined between the concrete shaft and the surrounding soil. The tangential coefficient of friction is fixed at 0.3 with an isotropic directionality. The normal contact behavior is assumed to be “Hard”, but the separation after the contact is allowed (see Figure 17).

As stated in the ABAQUS Documentation [75], the result accuracy for surface-to-surface discretization is higher compared to the node-to-surface discretization method. Also, the Finite-Sliding tracking approach is the most general among the others and it includes the nonlinearity effects. One of the contact surfaces shall be a master and the other is a slave, so it is suggested to assign the surface with stiffer properties as the master.

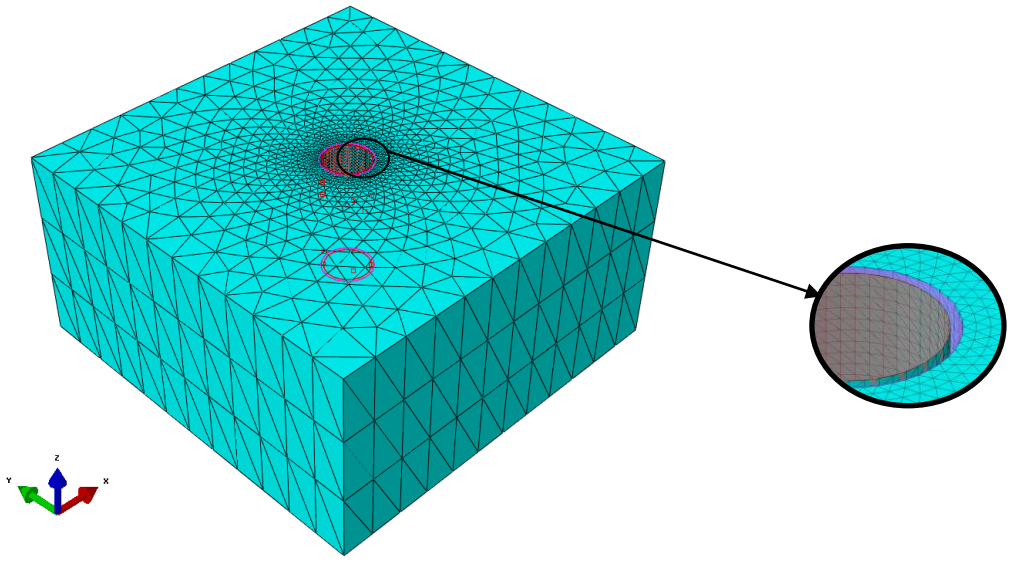

Figure 17. Soil Shaft Interaction

3.4 Element Types and Mesh Sensitivity Analysis

Figure 18 shows the model geometries of both the soil and the shaft. The soil surrounds the shaft from all sides and the bottom. A free mesh algorithm was adopted for the two parts. The concrete shaft was modeled as a conventional shell model using 3D triangular shell elements, and the soil was modeled using 3D tetrahedral solid elements as shown in Figures 19 and 20. Table 9 summarizes each element type and classification.

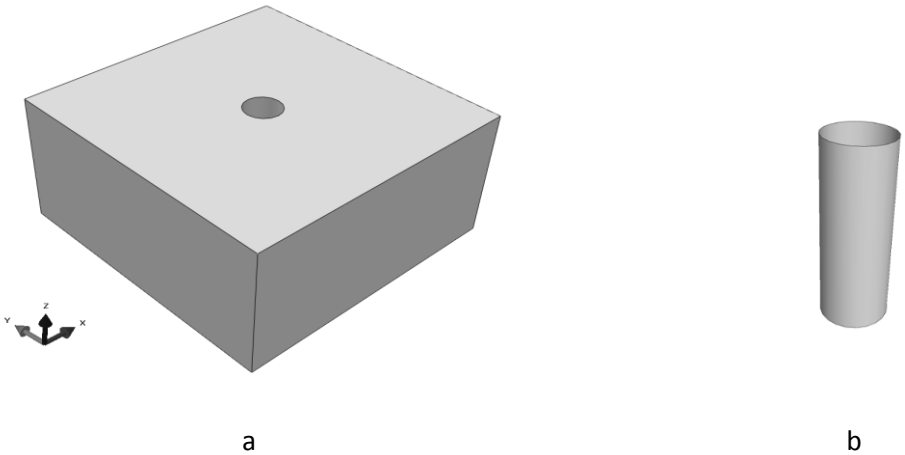

Figure 18. Full scale geometries (a) Soil Model with circular hole (b) Concrete Shaft Model

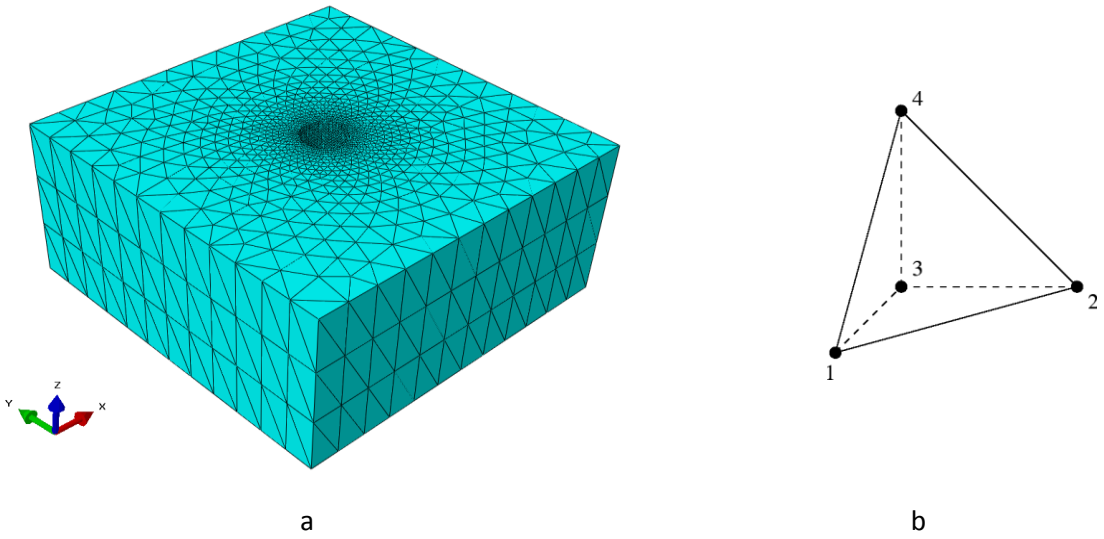

Figure 19. Soil (a) Free Mesh Algorithm with Tetrahedral elements (b) Free body diagram of tetrahedral element

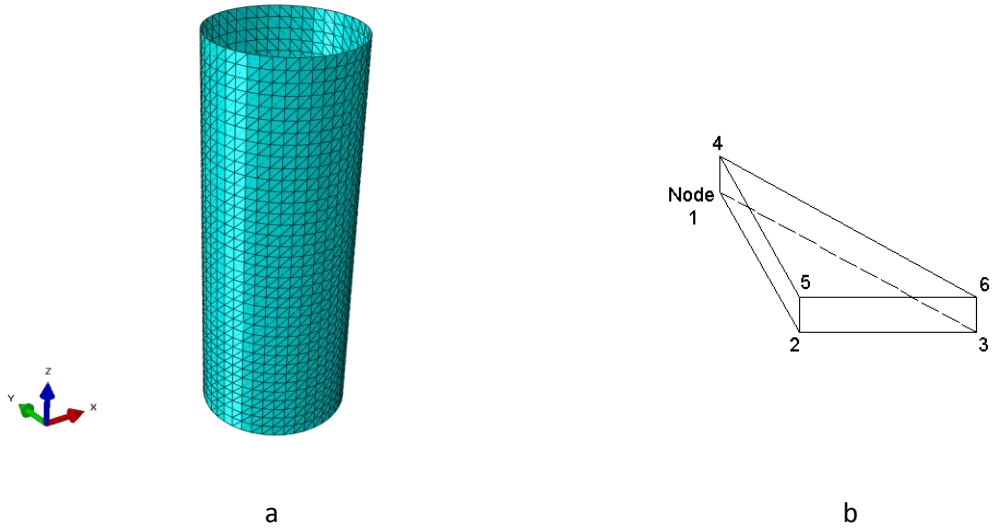

Figure 20. Shaft (a) Free Mesh Algorithm with Tetrahedral elements (b) Free body diagram of 3D conventional triangular element

Table 9. Summary of each element type and its classification

	Element type	No. of nodes	Element library	Family
Solid Element (Soil)	C3D4	4-node linear tetrahedron	Standard	3D Stress
Shell Element (Shaft)	S3	3-node triangular shell	Standard	Shell

Prior to the model's calibration, a mesh sensitivity analysis was conducted to select an optimum mesh with a proper number of elements to be used for the parametric study. For that reason, five mesh configurations shown in Figure 21were considered. The mesh

configurations 1 – 5 have approximate element sizes of 1.5m, 1.0m, 0.5m, 0.3m, and 0.2m consequently. An example of a mesh sensitivity analysis performed on the circular shaft is shown in Figure 22. The contour lines of radial displacements along the shaft surface obviously indicate that Meshes 4 and 5 provide similar numerical results compared to those of coarse mesh, so no more mesh refinement is required. The contour lines are smoother for smaller elements when using triangular elements [75]. The difference in error (e) is larger for coarser mesh, but insignificant for a very fine mesh. It was found that Mesh 4, with an approximate element size of 0.3, provides acceptable accuracy and minimal modeling analysis time.

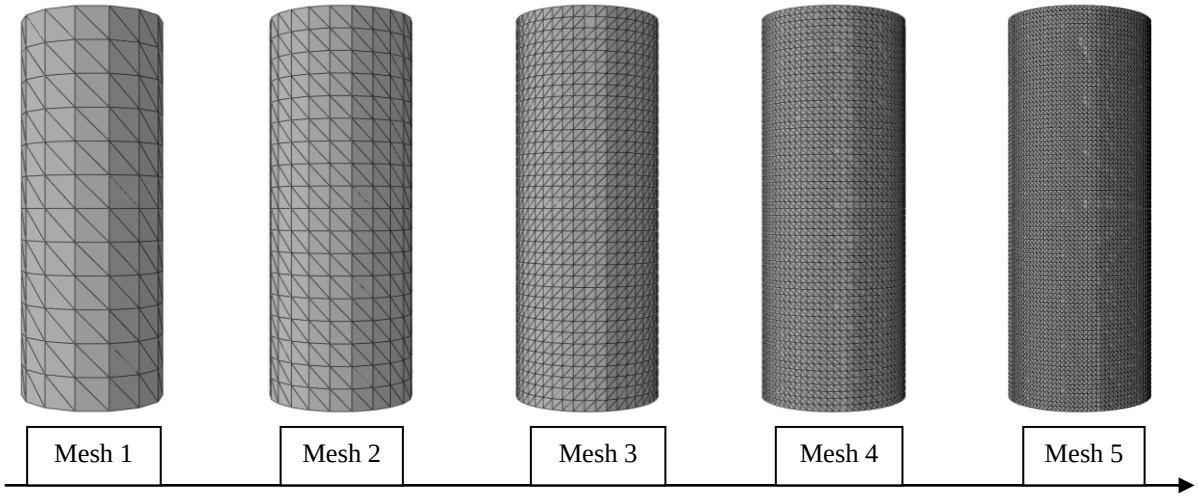

Figure 21. Different mesh configurations used for the analysis

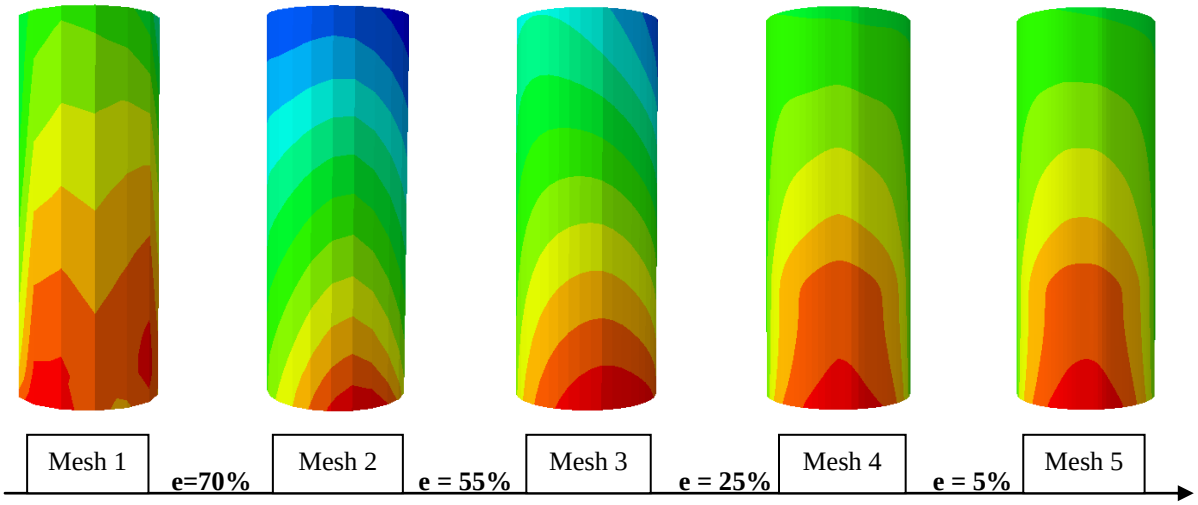

Figure 22. Displacement distribution on the shaft for different element sizes and the corresponding Difference Error

3.5 Model Calibration

This study outlines the design methodology, installation procedures and verification techniques used for the secant pile compression ring that is already implemented in Waterloo Landfill Pumping Station No. 2. This compression ring has a 6m diameter and 20m deep shaft with a depth of excavation inside the shaft equal to 18.2m. The monitoring data obtained experimentally for this shaft were utilized in this study to verify the present FE model. Figure 23 depicts the details of shaft layout and subsurface conditions. Several images depicting various stages of the shaft construction were also presented in Figure 24. Table 10 summarizes the soil and concrete properties assumed in the design.

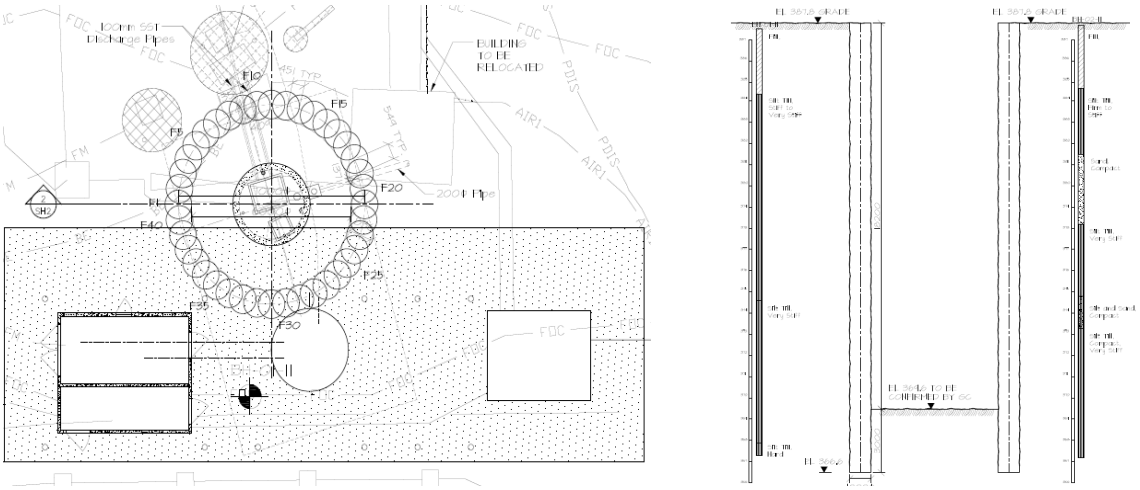

Figure 23. (a) Plan view of the shaft, and (b) Cross section of the shaft

a

b

c

Figure 24. Excavation stages (a) June 3rd (8m) (b) June 7th (13.5m) (c) June 13th (18.2m)

During the construction of walls, verticality was the major concern since the compression ring behavior can only be maintained as long as the uniformity in the wall thickness is maintained, which is only possible with very tight vertical installation tolerances. Thus, the approach described below was followed in order to maintain verticality. The circular caissons were installed using a Delmag 28 hydraulic drill rig equipped with a 1m diameter leffer casing system. To ensure verticality, a concrete guide was cast prior to commencement of vertical drilling. The guide wall was 1.2m wide by 0.76m deep with 1025mm holes formed in it to ensure the leffer casing was held in the right position. To increase vertical tolerance, the casing was deployed ahead of the auger. The caissons were installed in an alternating drilling sequence, making sure that there was either concrete or soil on either side of the casing to increase stability as the materials

on either side of the casing were of similar stiffness. A clamshell digger was used for the excavation of the shaft. The shaft was excavated symmetrically to minimize differential loading. The crane mounted clamshell differ was kept back 4.5m from the edge of the hole and worked off of timber mats to ensure stability. The overlapping of piles was 0.45m, which resulted in a wall thickness of 0.84m. Inclinometers were installed on two locations on the opposing sides of the walls. The readings in the radial and circumferential directions were recorded as an average of the two passes.

Table 10. Summary of material properties used in the shaft design

	Saturated Unit Weight (kN/m^3)	Effective Angle of Internal Friction (degree)	Elastic Modulus (MPa)	Poisson's Ratio	Wall Soil Interface Friction Ratio
Cohesive soil	22	27	40.6	0.35	0.5
Concrete	25	-	15000	0.25	0.5

3.5.1 Verification with Experimental Results

Displacement verification:

The deformations on the wall under external radial pressures were calculated using the FE method. The changes in the shaft diameters calculated using the FE model were compared with the monitoring results. A good agreement between the numerical and monitoring results was observed and the maximum changes in shaft diameter were around 0.2mm. The results of model calibration indicated that the FE model was able to replicate the soil-structure-interaction taking place between the secant pile wall and surrounding soil.

3.5.2 Verification with Analytical Results

Lateral earth pressures verification:

Similarly, the lateral earth pressure results predicted by the FE models were compared with the analytical calculations. The analytical approach is explained by the following equation:

$$q_{lateral} = K \,.\, \gamma \,.\, z \tag{21}$$

where q is the lateral earth pressure (kPa), γ is the soil unit weight ($\gamma = 21.5\frac{kN}{m^3}$), z is the depth $(z = 0 - 18\,m)$, and K is the lateral earth pressure coefficient defined as follows:.

$$K = 1 - sin\emptyset \tag{22}$$

where the soil friction angle $\emptyset$ is taken as 30^o. The lateral earth pressure values were plotted along the shaft depth in Figure 25.

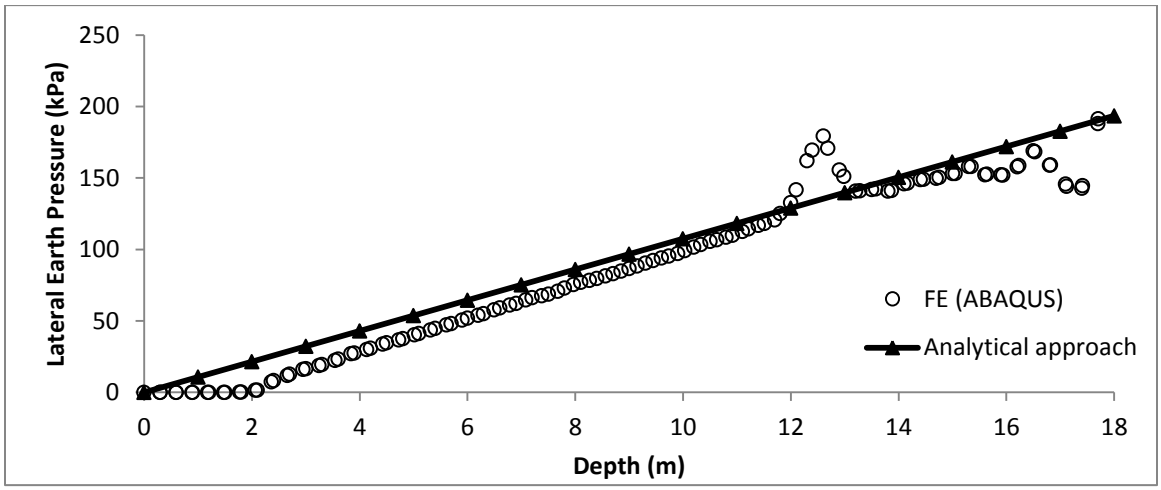

Figure 25. The lateral earth pressure values along the shaft depth

The maximum lateral earth pressures in both the analytical and FE analyses were around 200 kPa at 18m depth. The pressure distribution varied linearly along the shaft depth except for a small jump that occurred at about one third of the total shaft height from its base. The jump may be attributed to numerical instabilities existing in the FE simulations.

Circumferential stresses verification:

The circumferential stresses represent the hoop stresses through the circular wall thickness. The analytical solution approach was compared with the FE results. The hoop stresses were calculated analytically using the following equation [70]:

$$\sigma_2 = \frac{-q.a\,(b^2 + x^2)}{x^2\,(a^2 - b^2)} \tag{23}$$

where σ_2 is the circumferential stress(Mpa), a is the outer radius $(a = 3.84\,m)$, b is the inner radius $(b = 3\,m)$, and x is the point of interest $(x = 3\,m)$. The analytical and FE stress values were plotted along the shaft depth in Figure 26.

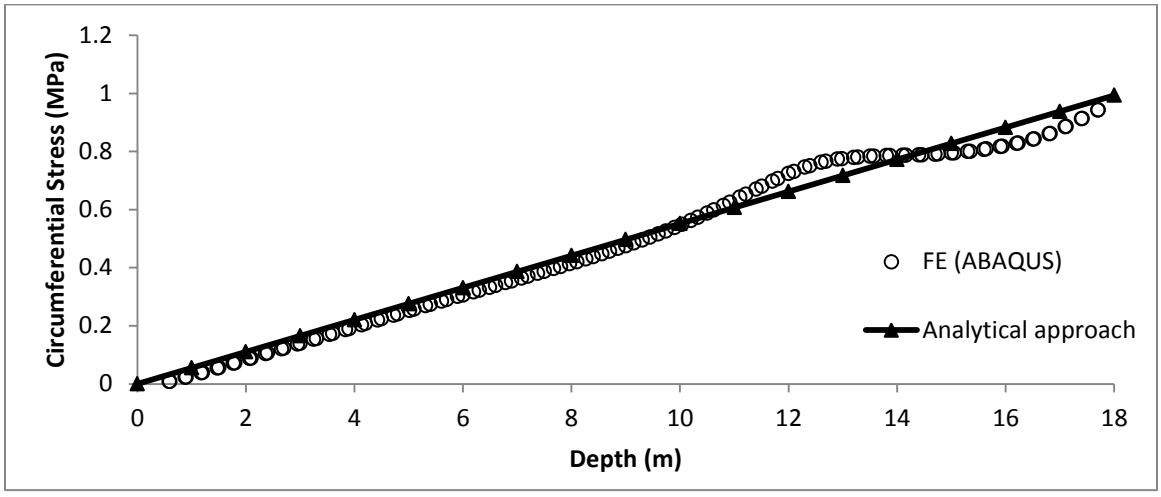

Figure 26. Variation of the circumferential stresses along the shaft depth

It is very clear that the circumferential stresses increase with the shaft depth, where a maximum value of 1 Mpa was recorded at the shaft base. The circumferential stress represents the compression effect on the wall thickness which is basically resisted by the compressive strength of the concrete.

4. Results & Discussion

The verified FE model developed in the previous chapter is further utilized in this work to study the interaction between the secant shafts and the surrounding soil. Various practical aspects related to the design of these systems were investigated, which included the assumptions related to earth pressure distribution along the depth of the shaft and the horizontal arching mechanism, impact of wall deformations on the earth pressures exerted on the wall, the three dimensional nature of the distribution of surcharge pressures on the circular walls considering various surcharge-to-shaft distances and surcharge widths, investigation of the interaction between vertical circular shafts and the surrounding soil with consideration of holes on the shaft walls, and the impact of the sloping bedrock conditions and type of granular soil on the abovementioned.

4.1 Earth Pressures on Circular Shaft

The earth pressures determined in this study were presented as normalized earth pressures ($p/R\gamma$) against various normalized depth ratios (H/R) in order to be consistent with the depiction of similar data in the literature. The results were presented for up to a maximum normalized depth ratio of H/R = 8, which covers most practical shaft dimensions. The lateral earth pressures calculated using the finite element method were plotted against the values proposed by Terzaghi [8], Brezantzev [9], Prater [10], and Cheng & Hu [76].

Figures 27 and 28 show the normalized earth pressures in soil strata with $\emptyset = 30^o$ and $\emptyset = 40^o$, respectively. The results indicate that the calculated earth pressures can be represented by the at rest pressure distribution for $\emptyset = 30^o$ soil. However, the earth pressures increased from an active condition for (H/R) between 0 and 3, to an at-rest condition up to (H/R) of 8 for $\emptyset = 40^o$ soil. For both cases of $\emptyset = 30^o$ and $\emptyset = 40^o$, the earth pressure trends were slightly irregular at shallow depths. This is considered to be numerically driven and caused by the constitutive model utilized in the numerical analyses. The earth pressure distribution is known to be strongly influenced by the stiffness of the soil. However, a constant stiffness value is considered in the analyses and

the constitutive soil model which considered to be the reasons for this local trend. In both cases, the finite element results were higher than the normalized earth pressures reported in the literature. This difference is due to the fact that the circular shaft exhibited compression ring behavior under balanced earth pressures and resultant wall movements were not large enough to reduce the lateral stresses from at-rest conditions to active conditions for the shaft diameter, thickness and material properties considered in this study. Figure 29 shows normalized lateral earth pressures for three different soil types (see Table 6). The models with three different soils exhibit similar pressure change trends with depth. The results depicted in Figures 27 and 28 indicated that the practical shaft dimensions and material properties resulted in very small wall deformations that were not enough to generate active earth pressure conditions and as expected no yielding of the retained soil was observed due to these small deformations. For all analyzed cases, the simulated deformations remained well below the deformation criterion recommended by Fujii et al. [77], Imamura et al. [78], Herten and Pulsfort [16] and Chun and Shin [79] for dense sands and the one recommended by Tobar and Meguid [14] for loose sand.

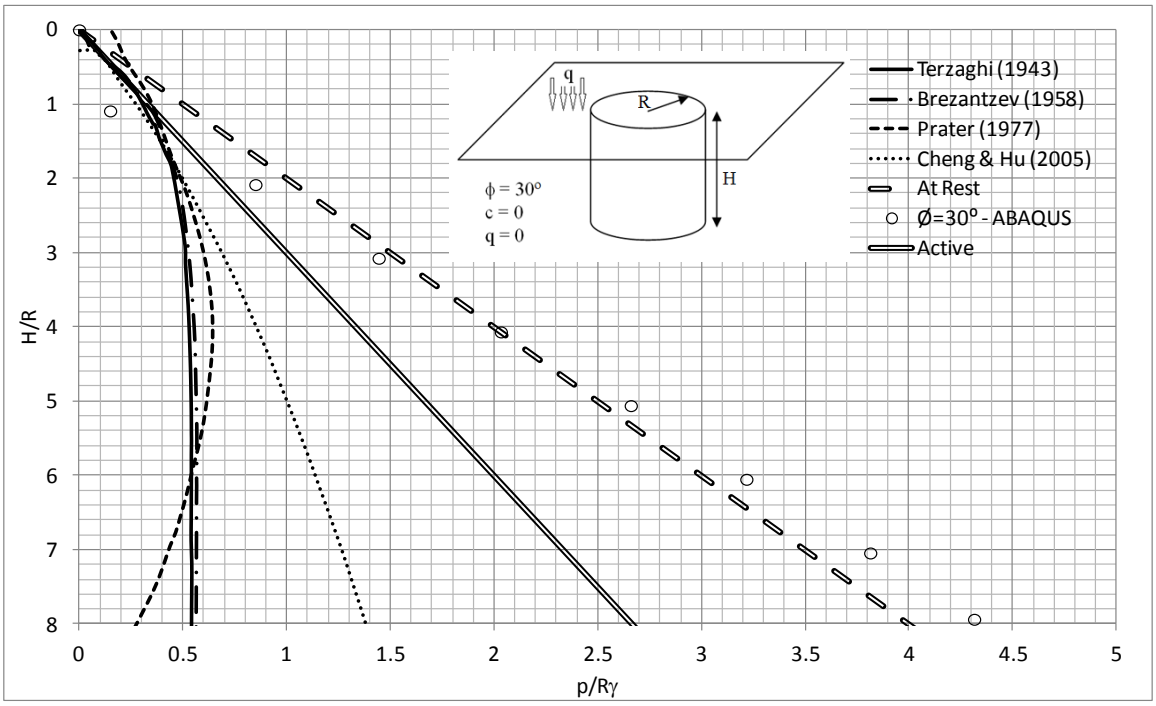

Figure 27. Normalized earth pressure distribution on shaft in cohesionless soil (Ø=30°, no surcharge)

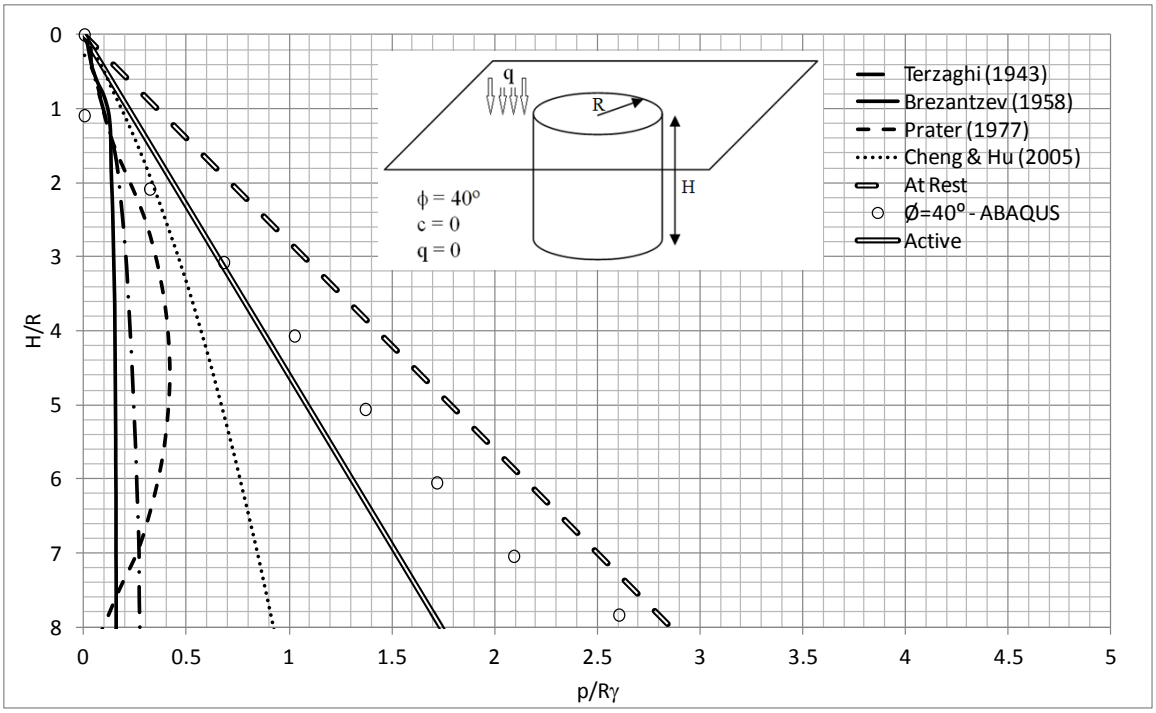

Figure 28. Normalized earth pressure distribution on shaft in cohesionless soil (∅=40°, no surcharge)

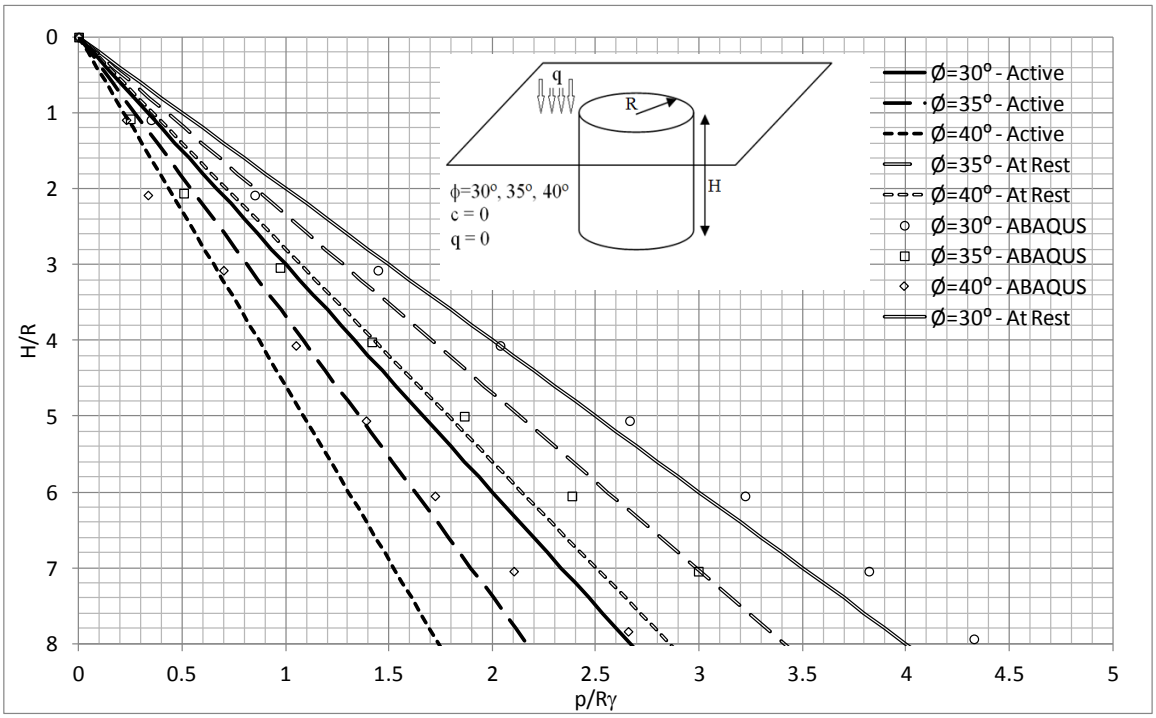

Figure 29. Earth pressure distribution for different soil properties (∅=30°, 35°, 40°)

4.2 Effect of Hole Excavation on the Stresses in the Circular Shaft

The excavation of a hole in a circular shaft resulted in compressive stresses that were larger than what would be expected in a symmetrically loaded circular shaft (compression only). The tensile stresses also occurred in the vicinity of the holes after the excavation of the holes. The stress concentration factors (σ_{max}/σ_{11}) were calculated and presented against the (r/R) ratios.

4.2.1 Single Hole on the Shaft

Figure 30 shows the stress concentration factors calculated at the top of and on the side of the excavated hole for various (r/R) ratios. The infinite plate solution yields a theoretical value of 3.0 for the stress concentration factor in the compression zones above the hole and a value of 1.0 for the tensile stress concentration factor on the sides of the hole. These values were plotted in Figure 30 along with the results of finite element analyses. As can be observed from Figure 30, the analytical solution for determining the stress concentration factor for a hole on an infinite plate gives constant values for compression and tension. The FE results depicted in Figure 30 also show that the stress concentration factors were a function of (r/R) ratios for curved surfaces such as the walls of the circular shaft. As the (r/R) ratio approaches 0, the stress concentration factors converge to the theoretical value of 3 for the compression. Stress concentration factors reduce to values as low as 1.5 for large (r/R) ratios. The stress concentration factors for tensile stresses on the sides of the hole were calculated as 1.3 for low (r/R) ratios and as high as 2 for large (r/R) ratios. The stress concentration factors calculated for tensile stresses were larger than the theoretical value of 1 reported for an infinite plate and thus they were unconservative. The difference between the theoretical results and simulated results using the FE method has two causes. The first is that the load applied in the FE analyses was a uniformly increasing pressure along the depth of the circular shaft as opposed to the concentric force acting on the plate edges in the infinite plate solution. This results in compressive concentration factors decreasing with the increase of the (r/R) ratios as the total shaft surface area decreases. The second reason is that the circular openings are on a curved surface as opposed to a straight plate. Because of that, the

tensile concentration factors at the hole sides increase as (r/R) ratios increase due to the bending effect on the sides of the holes.

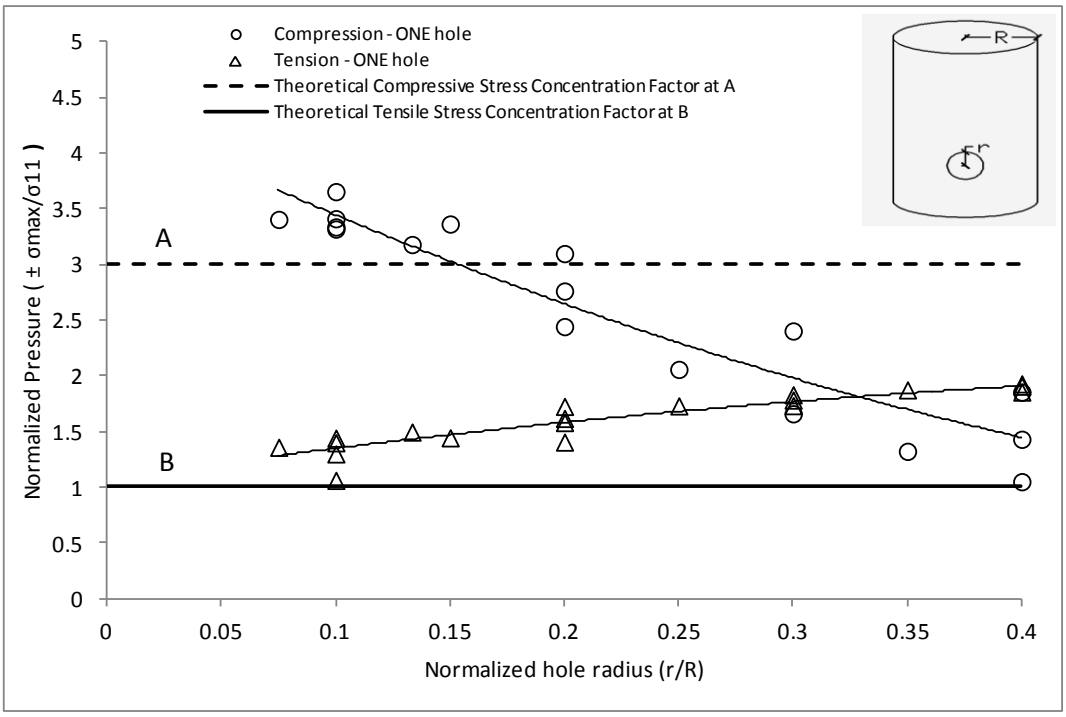

Figure 30. Stress concetration factors for a single hole on circular shaft. Theoretical solution of hole on plate vs. finite element results

4.2.2 Multiple Holes on the Shaft

Figure 31 shows the stress concentration factors calculated for compression (on top) and tension (on the side) zones of the hole excavated on the wall of a circular shaft for various normalized hole radius (r/R) values considering two identical holes.

The FE results depicted in Figure 31 show that the stress concentration factors were a function of normalized hole radius (r/R) for curved surfaces such as the walls of the circular shaft. As the (r/R) ratios approach 0, the stress concentration factors approached 2.5 for the compression. Stress concentration factors decrease to values as low as 1.3 for large values of (r/R) ratios. The stress concentration factors for tensile stresses on the sides of the hole were calculated as 1.7 for low (r/R) ratios and as high as 2 for large (r/R) ratios. It can be observed from the results in Figure 31 that the existence of a second hole

on the shaft wall reduced concentration factors for compression and increased them for tension.

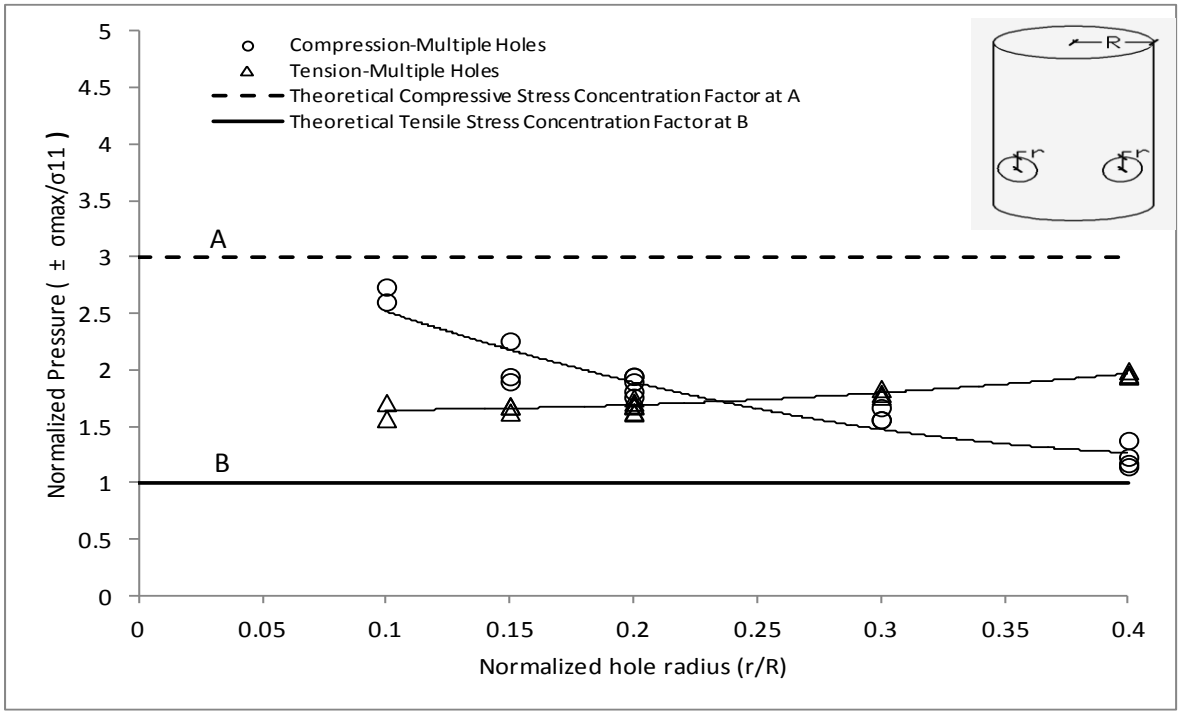

Figure 31. Stress concentrations factors for multiple holes on the circular shaft. Theoretical solution of hole on plate vs. finite element results

The effects of the distance between the holes on the stress concentration factors were also studied parametrically. Figure 32 depicts the variation of stress concentration factors with the hole-to-hole distance. The results indicate that the values of stress concentration factors were almost independent of the hole-to-hole distance.

The analyses that investigated the impact of hole excavation on the wall of a circular shaft resulted in stress regimes that differed significantly from what would be expected for a compression ring. The reason for the reduction of compressive concentration factors in the case of multiple holes is that the principle stresses within the shaft walls were being arched around the other hole, which reduces the initial hoop stresses that would be the base for the stress concentrations around the hole under consideration. The increases in tensile stresses also result from the same mechanism, which eliminates some of the compensating compressive stresses that would determine the net tensile stress.

Thus, the stress concentrations should be taken into consideration in the design of circular shafts with hole(s).

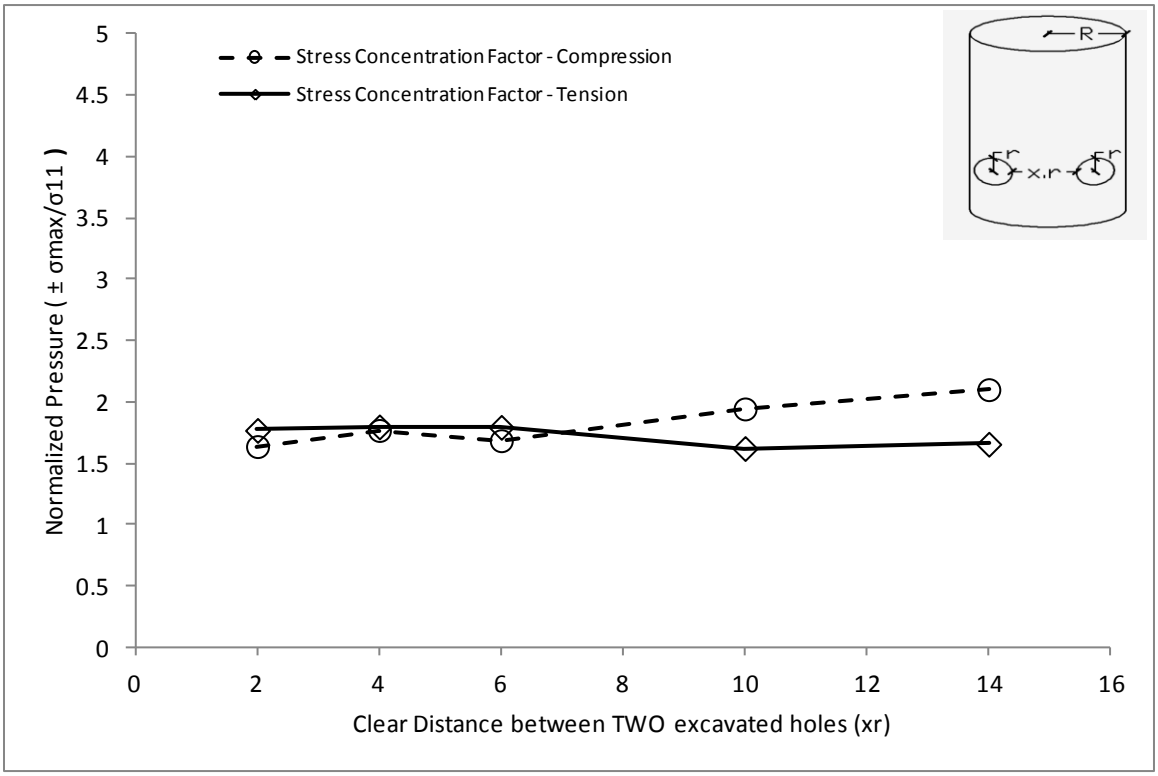

Figure 32. Effect of distance between holes on stress concetration factors for two holes on circular shaft

4.2.3 Effect of Shaft Boundary

The holes are typically excavated near the bottom of the shafts and the boundary effects on the stress concentration factors were studied. Figure 33 shows the effect of the distance between the hole and the lower boundary of the shaft and stress concentration factors for two different (r/R) ratios. The results indicated that there was almost no boundary effect. This can be explained by the compression ring behavior. The stresses in concentration zones are governed by the initial hoop stresses, and the distance to a hole has only a minor impact on these stresses unless special boundary conditions such as socketing to bedrock exist.

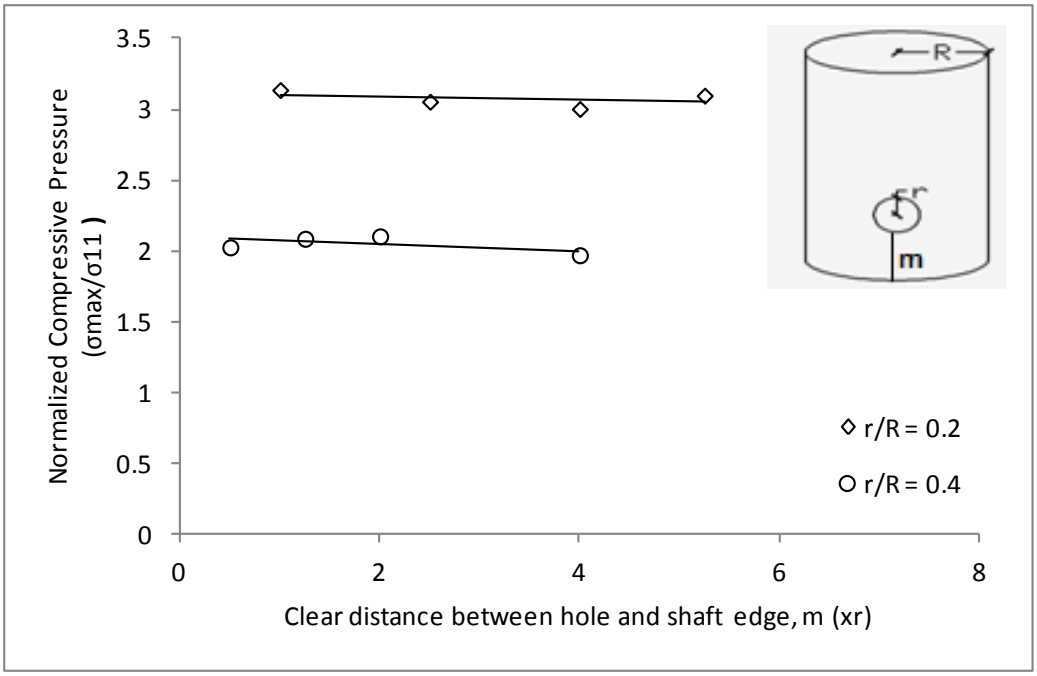

Figure 33. Effect of distance between hole and shaft boundary

4.3 Effect of Sloping Bedrock on the Stresses in the Circular Shaft

The existence of a sloping bedrock, where the secant pile wall circular shafts are typically installed if they are in reasonable depths, may result in wall stresses that would be significantly different from what would be expected from a symmetrically loaded circular shaft (compression only). Figures 34 to 36 depict the results of analyses of bedrocks inclined at 10, 20 and 30 degrees (cases 1, 2 and 3) along with the results of a plane bedrock case (0 degree). The results indicate that the circumferential stresses in the wall of a circular shaft were purely compressive and that they increased with increasing depth. However, significant variations were observed in the stresses with various inclinations of bedrock. For example, Figure 34 depicts the variation of circumferential stresses along axes 1, 2 and 3 for a bedrock sloping at 10 degrees (case 1). The results show that the maximum compressive stresses along axes 1, 2 and 3 remained below the maximum compressive stress of a plane bedrock (compression ring). The circumferential stresses in the shaft were observed to be almost fully compressive for case 1. Figure 35 depicts the variation of circumferential stresses along axes 1, 2 and 3 for a bedrock sloping at 20 degrees (case 2). The results show that the maximum compressive stresses

along axes 1, 2 and 3 remain below the maximum compressive stress of a plane bedrock case. However, at shallow depths and along axis 1 (side with deep soil) tensile stresses occurred. Figure 36 shows the variation of circumferential stresses along axes 1, 2 and 3 for bedrock sloping at 30 degrees (case 3). The results show that the compressive stresses that occurred along axis 2 exceeded the maximum compressive stress of the plane bedrock case significantly. On the other hand, significant tensile stresses occurred along axes 1 and 3. It was observed that the largest compressive stresses occurred along axis 2. Thus, it should be noted that the circular shafts that are located on sloping bedrocks with inclinations of 20 degrees and larger should be designed to account for both the increased levels of compressive stresses and the newly emerged tensile stresses resulting from the bedrock inclination. The large stress deviations occur because of the differential soil depths between the two shaft sides (axes 1 & 2). For an inclination angle of 20 degrees and more, the unbalanced loading caused by the soil resulted in significant tensile and compressive stresses on the shaft.

It is important to decode the interaction mechanisms that take place between the soil, bedrock and circular shaft in order to understand the reasons for the stress trends which are highly dependent on the bedrock inclination. An increasing bedrock inclination resulted in an increasing earth pressure situation along 1-3 axis due to the downward mobilization trend of soil along this axis. However, the earth pressure acting parallel to axis 2 remained unaffected from such movements. Thus, the increasing bedrock inclinations and resultant unbalanced pressures created deviations from compression ring behavior and resulted in tensile stresses. Unaffected axis 2 stresses tended to remain under compression due to soil confinement and passive resistance exerted on the exterior face.

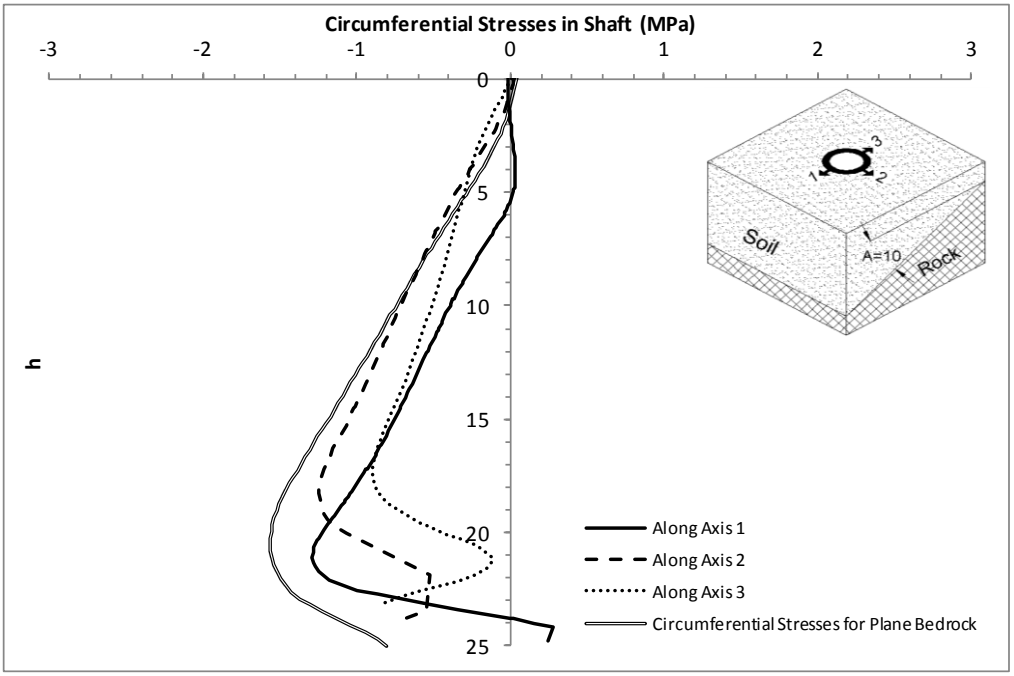

Figure 34. The circumferential stresses in the walls of circular shaft (Bedrock Inclination A=10°)

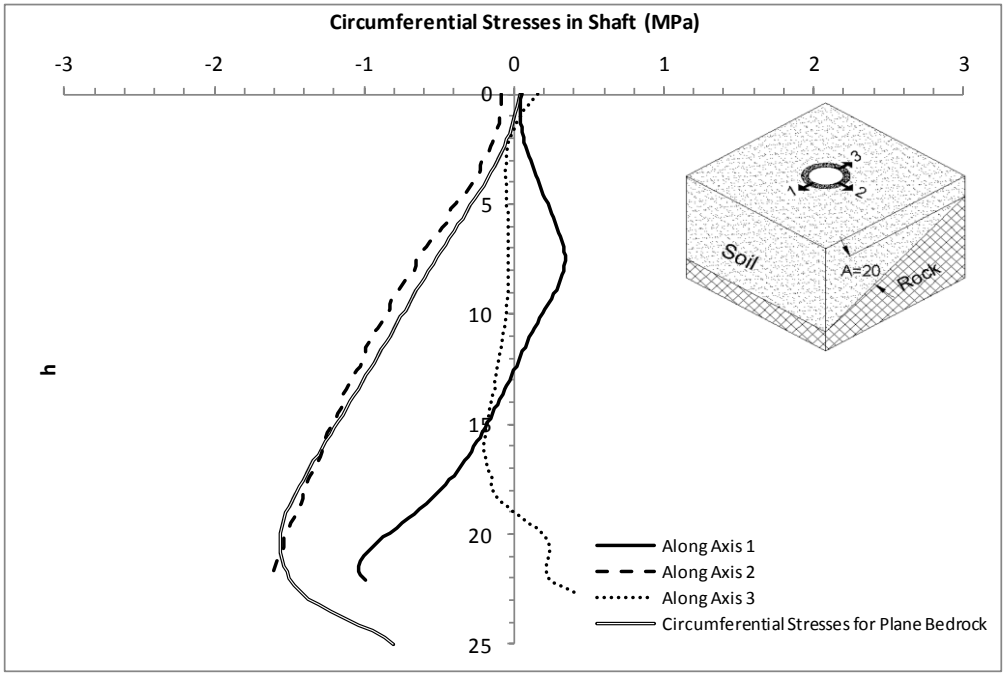

Figure 35. The circumferential stresses in the walls of circular shaft (Bedrock Inclination A=20°)

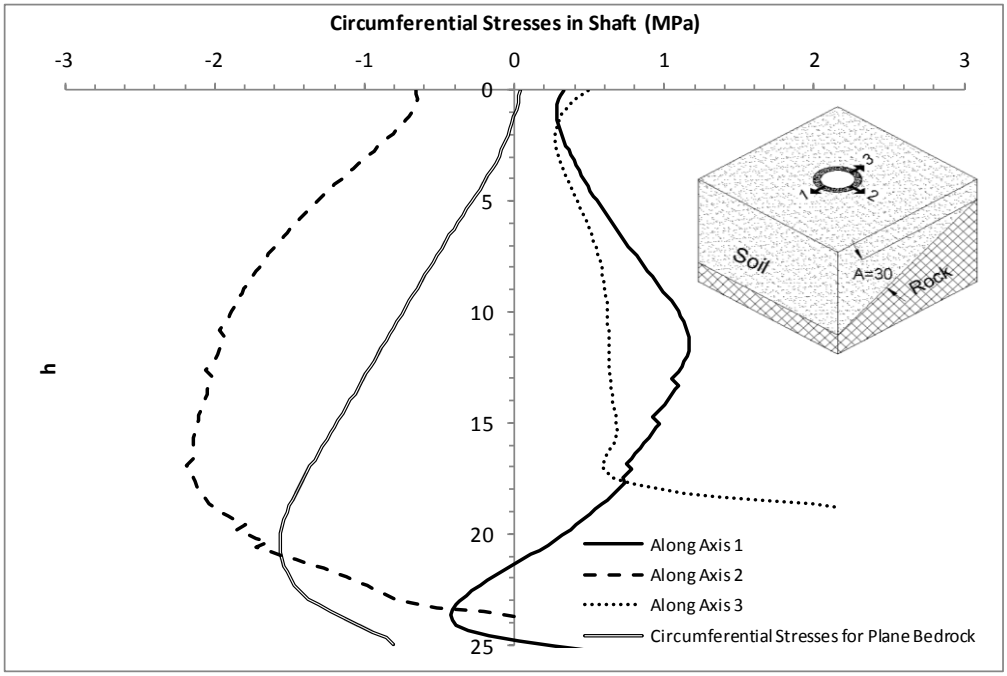

Figure 36. The circumferential stresses in the walls of circular shaft (Bedrock Inclination A=30°)

4.4 Effect of Surcharge on Secant Pile Circular Shaft

The contact pressures at the interface between the circular shaft and soil were presented as a percentage of applied surcharge pressures (σ/q) against the depth of shaft (H) in this section. The maximum shaft depth of 25m was considered in the parametric analyses. The theoretical earth pressures were calculated in accordance with Laba and Kennedy [80] assuming a straight wall rather than the walls of a circular shaft (plane strain conditions). Two shaft radii, R = 3m and 5m, were considered in the analyses.

4.4.1 Effect of Surcharge Width (W)

Figure 37 shows the distribution of lateral pressures due to surface surcharge with various widths of surcharge load footprints. The surcharge widths varied from 3m, which was a narrow surcharge that was representative of a small size crane pad, to a long surcharge (48m), which was more representative of an embankment type of loading near the shaft. The length of the surcharged area was larger than the shaft depth for all cases.

As can be seen from Figure 37, which compares the cases with W = 3m and W = 48m, the maximum pressures acting on the shaft wall increased with the increasing width

of the surcharged area, W. This is expected since the total applied pressure increased significantly. This result indicates that at least a 60% increase took place in the maximum surcharge induced lateral pressure acting on the shaft wall between the cases of W = 3m and W = 48m. The impact of W on the maximum lateral pressures on the wall was independent of the shaft radius. However, the surcharge distance from the circular shaft, D, and soil friction angle,∅, were seen to have a significant impact on the effect of W on the maximum pressure. Increasing values of D resulted in significant decreases of the maximum pressures for W = 3m cases, whereas the W = 48m cases were not significantly impacted. However, it is expected to have an impact on maximum pressure values at W = 48m when D is large enough. Results also show that the increasing soil friction angle, ∅, and stiffness resulted in a larger difference between W = 3m and W = 48m cases. The results depicted in Figure 37 show that the maximum surcharge induced lateral pressure on the wall remained below the analytical estimates assuming plane strain conditions. Figure 38(a) illustrates how the maximum lateral pressure on the wall changes with the change in W. An incremental increase in the maximum lateral pressures with increasing W was observed for a select case that was representative of all other cases analyzed in this study. The results also indicate that the change of the maximum pressure values have a non-linear relationship with W values.

The distribution of pressures deviates from the theoretical distribution at larger depths as the analyses at larger depths exceeded the theoretical values. Figure 38(b) presents the variation of maximum surcharge pressure with W, and clearly shows that the changes in the pressure values were negligible beyond the maximum value of W considered in this study. The impact of W on the maximum surcharge pressure is based on the fact that the increasing W creates a wider angular zone of impact as well as a larger magnitude since the lateral pressures due to surcharge at a given point is the superposition of surcharge pressure at various distances from the axis of the shaft.

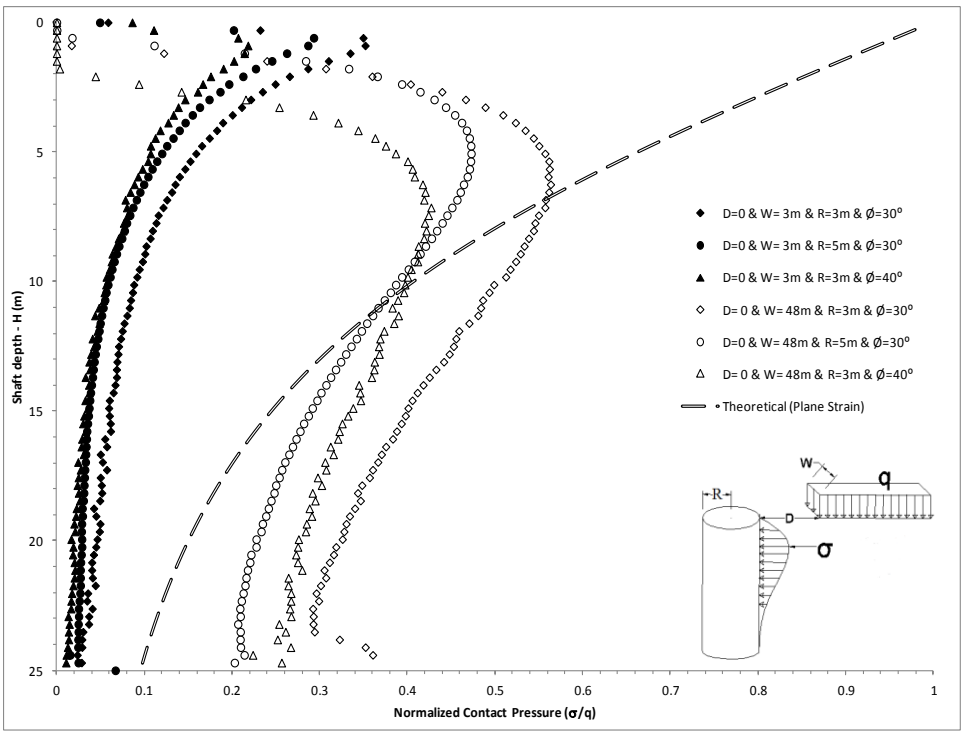

a

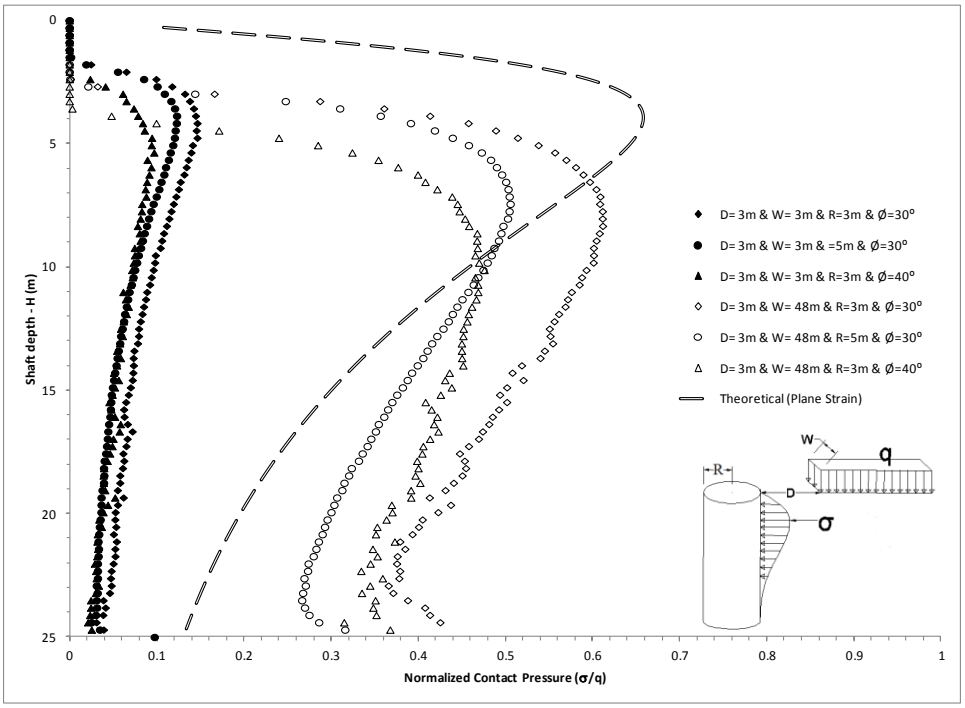

b

Figure 37. The effect of width of surcharge footprint, W, on the maximum surcharge pressure on the wall (a) D = 0m (b) D = 3m.

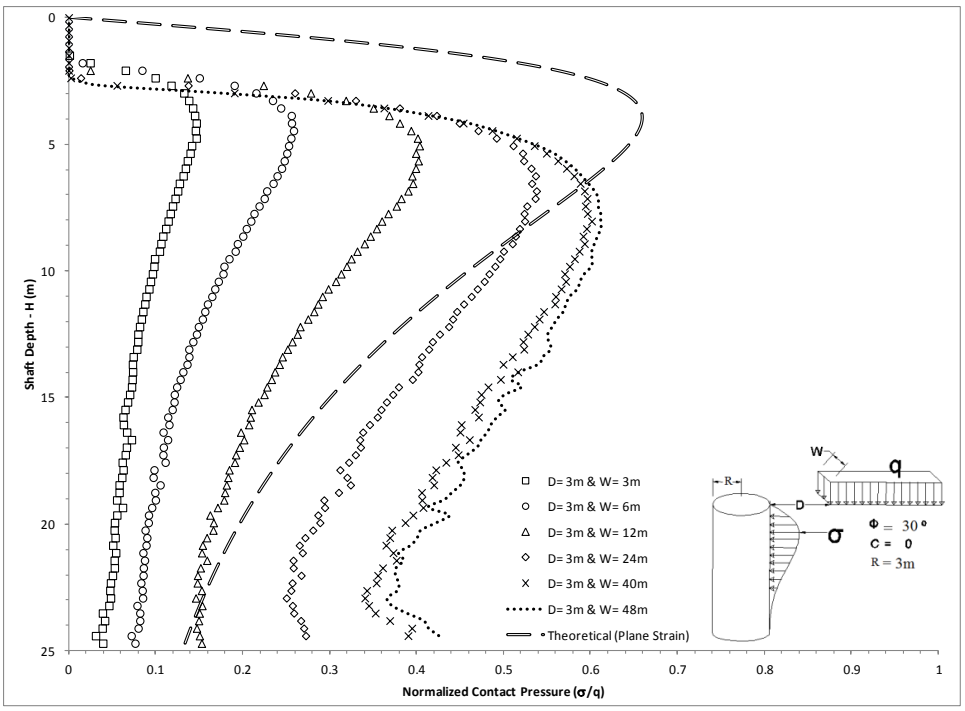

a

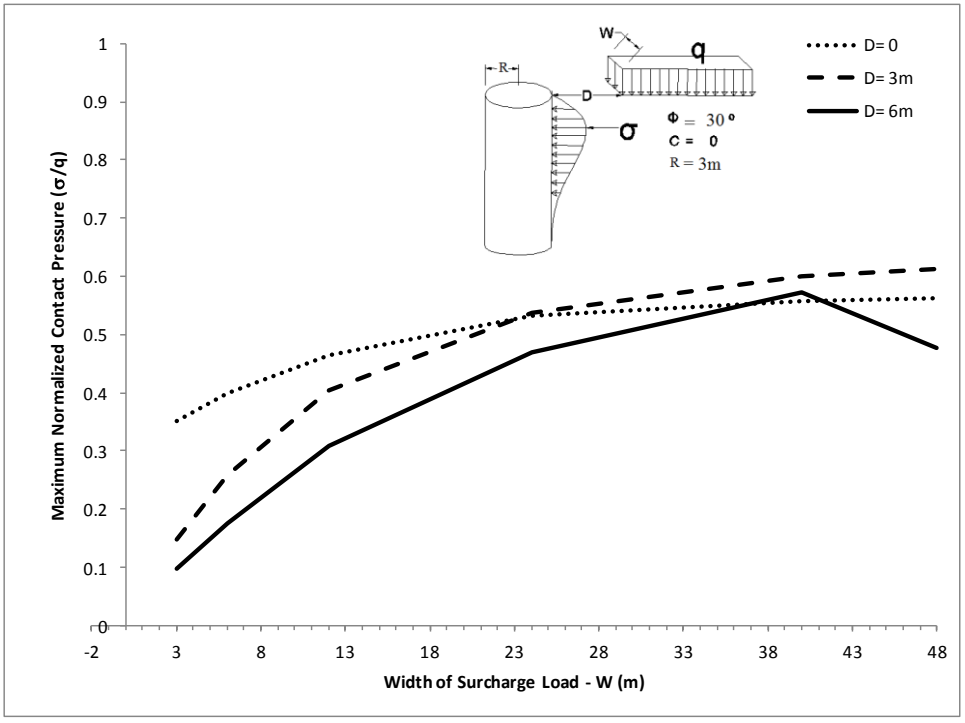

b

Figure 38. Variation of maximum surcharge pressure on the wall with W

4.4.2 Effect of Surcharge Distance (D)

The effect of the distance of surcharge to the shaft can be seen in Figure 39, which shows the distribution of surcharge pressures located at distances of 0m, 3m and 6m from a shaft with R = 3m. Our results indicated that the maximum pressure for the case with D = 0 remained significantly below the analytical estimate (53%). The circular cross-section of the shaft had an impact on the maximum lateral surcharge pressures due to the horizontal arching mechanism. The maximum stress was calculated as 91% of the theoretical value when D was 3m. The calculated maximum pressure exceeded the theoretical value by 16% when D was 6m. For all three cases, the results indicated that the calculated stresses were larger than the theoretical estimates at larger depths. The effect of D on the maximum stresses exerted on the wall for other shaft radii and soil properties was seen to have a similar trend to those shown in Figure 39 with different magnitudes. The results summarized in Table 11, which also includes the results of Figure 39, indicate that the largest pressure occurred for D = 3m. However, it should be noted that the differences caused by D are small from a design perspective.

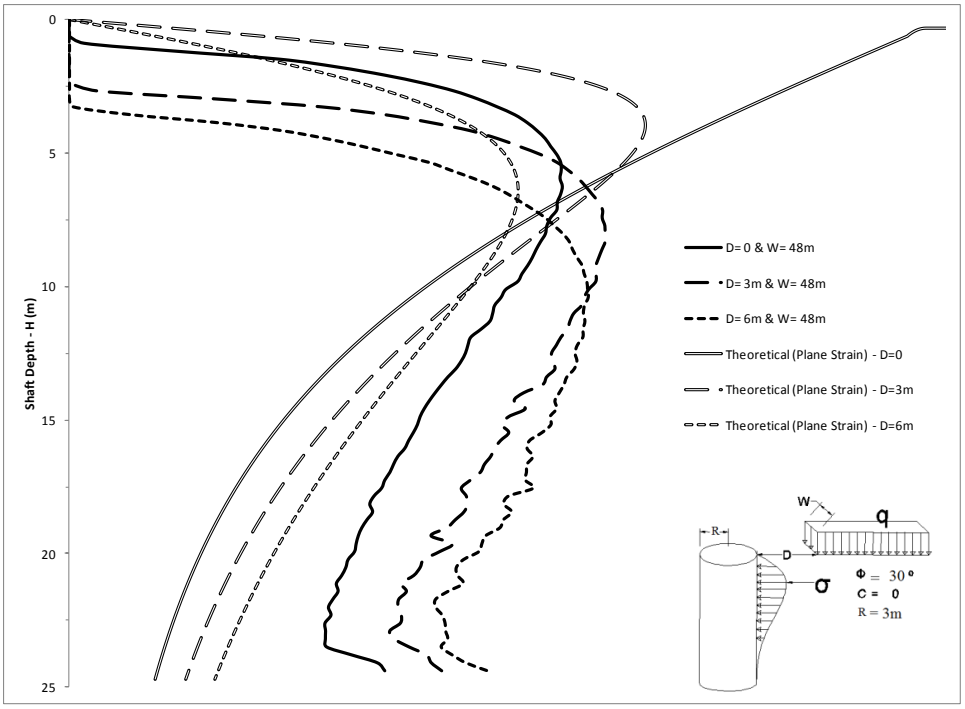

Figure 39. Variation of maximum surcharge pressure on the wall - effect of D (R = 3m and ∅=30°)

4.4.3 Effect of Shaft Radius (R) and Soil Type

Figure 40 illustrates the influence of shaft radius on the maximum surcharge pressures on the wall for a shaft case with D = 3m. The results showed that the maximum surcharge pressure on the shaft walls decreased with an increase of the shaft radius. For the cases where the shaft radius is large, horizontal arching takes place around a hypothetical wedge, the size of which is determined by the diameter of the shaft. The increasing shaft radius increases the size wedge shields of the shaft and reduces the surcharge pressures. For example, the maximum surcharge pressure on the wall for a shaft where R = 3m was 22% larger than that of an R = 5m shaft for Soil 1. The values for Soil 3 also showed similar reductions.

The type of soil was shown to have a significant impact on the distribution of surcharge pressures on the shaft wall. As can be seen from Figure 40, a 29% reduction in the surcharge pressures took place when the soil type was changed from Soil 3 to Soil 1 since the soil Poisson's ratio had the greatest effect on the pressure values. The effect of shaft radius and soil type on the maximum surcharge pressures can be observed in Table 11.

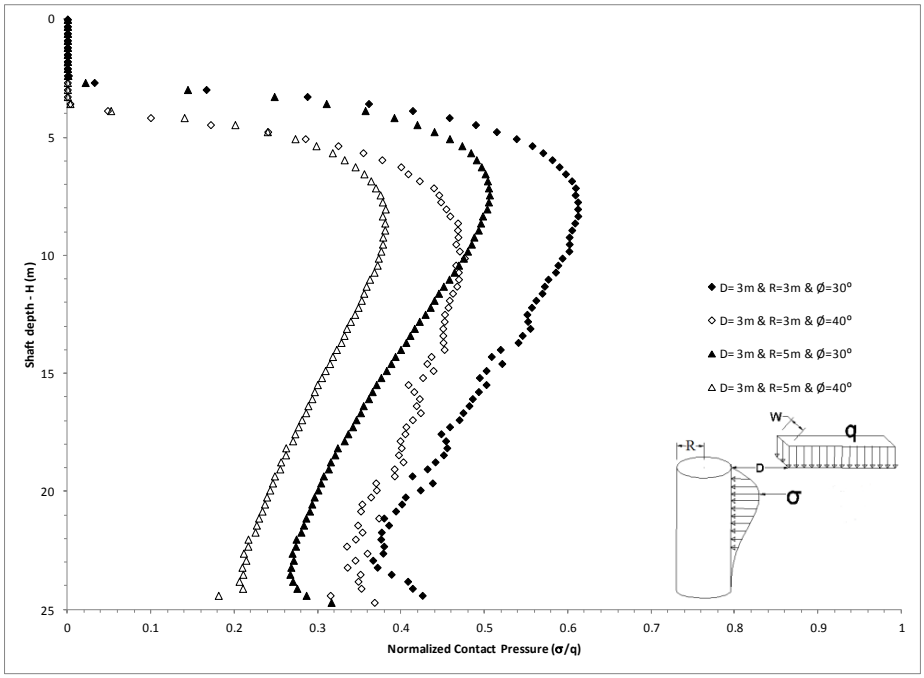

Figure 40. Variation of maximum surcharge pressure on the wall - effect of R and ∅

Table 11. Maximum surcharge pressures on the wall for various soil and shaft conditions

Soil Friction Angle (deg)			Soil Friction Angle (deg)	
30			40	
Shaft Radius (m)			Shaft Radius (m)	
D (m)	3	5	3	5
0	54.00%	42.00%	48.00%	31.00%
3	61.00%	46.00%	50.00%	37.00%
6	59.00%	45.00%	47.00%	36.00%

4.4.4 Distribution of Pressures in Horizontal Plane

The vertical distribution of maximum surcharge pressures on the shaft wall was discussed in detail earlier. However, considering the peak values only is not sufficient to define the loads on the shaft in three dimensions. The variation of the maximum pressure within the horizontal plane, where it takes place, should be known in order to fully define the applied load that would allow the use of analytical solutions to calculate the stresses in the wall sections. Determination of the radial extent to which the surcharge pressures reach is an important step in the design process.

Figures 41(a) to (d) show the radial extent of the horizontal distribution of surcharge pressures for various shaft radii and soil types. The results reveal that the dissipation angle (θ), the angle to which the surcharge pressures reach, increased with increasing values of W because the three dimensional pressure distribution propagates along the circular wall. The increasing values of D, on the other hand, had a minor reducing effect on θ. In contrast, the dissipation angle (θ) was observed to decrease significantly when the soil type was changed from Soil 3 to Soil 1 since the pressure distribution is related directly to the Poisson's ratio. The soil type was seen to have a major impact on the horizontal distribution of pressures on the shaft. Figure 42 depicts the dissipation angles for a shaft with R = 3m for Soil 3 and Soil 1 (See Table 6). The results indicated that the dissipation angles decreased significantly when the soil type was changed from Soil 3 ($\emptyset = 30^o$) to Soil 1 ($\emptyset = 40^o$). This reduction is more pronounced for large values of W.

Figure 43 shows the variation of dissipation angles with shaft radius (R). The results indicated that the dissipation angles were almost unchanged when shaft radius (R) was changed, particularly for large values of W (parallel embankment loading).

The results summarized above show that a parabolic distribution can be assumed for the determination of in-plane distribution of surcharge pressures within a horizontal plane.

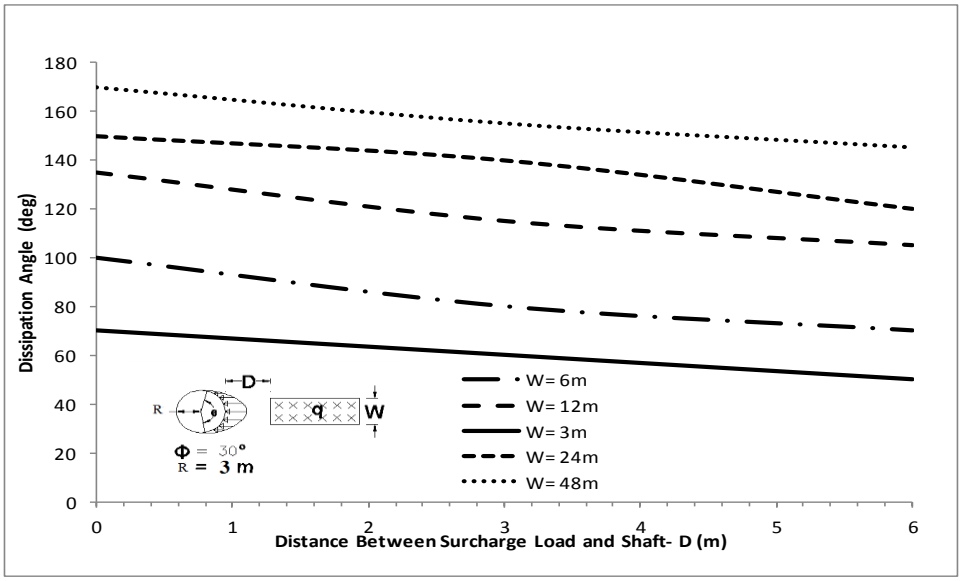

a

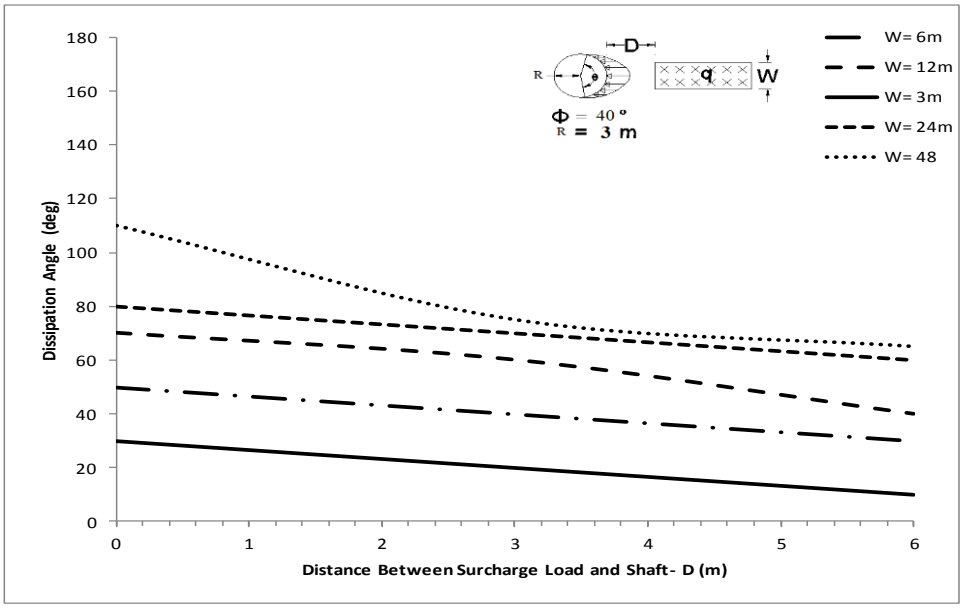

b

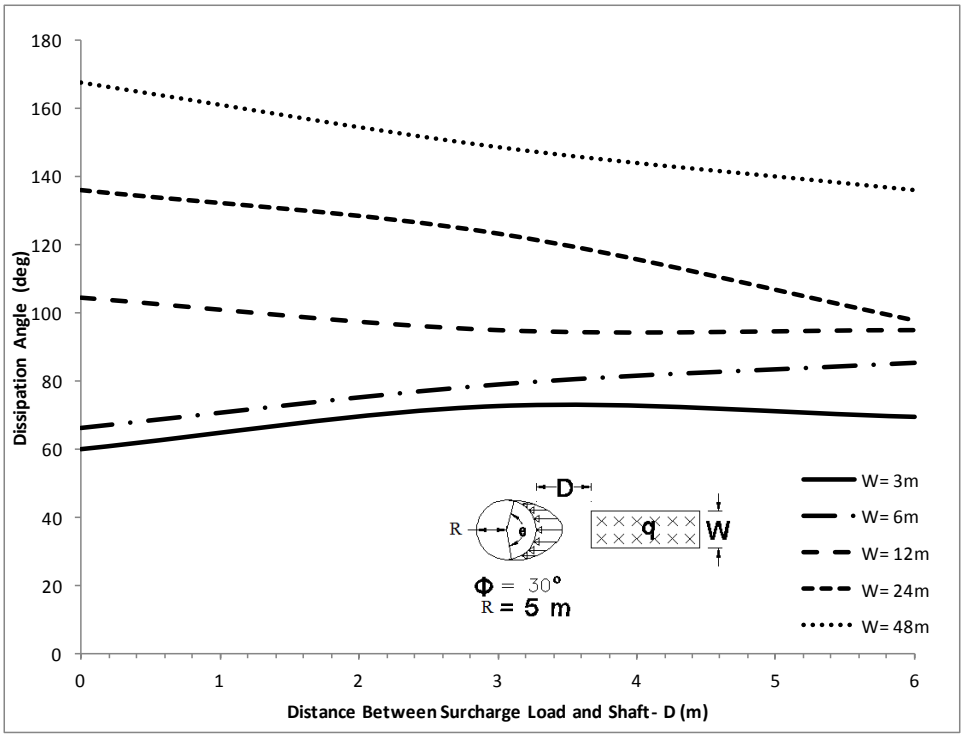

c

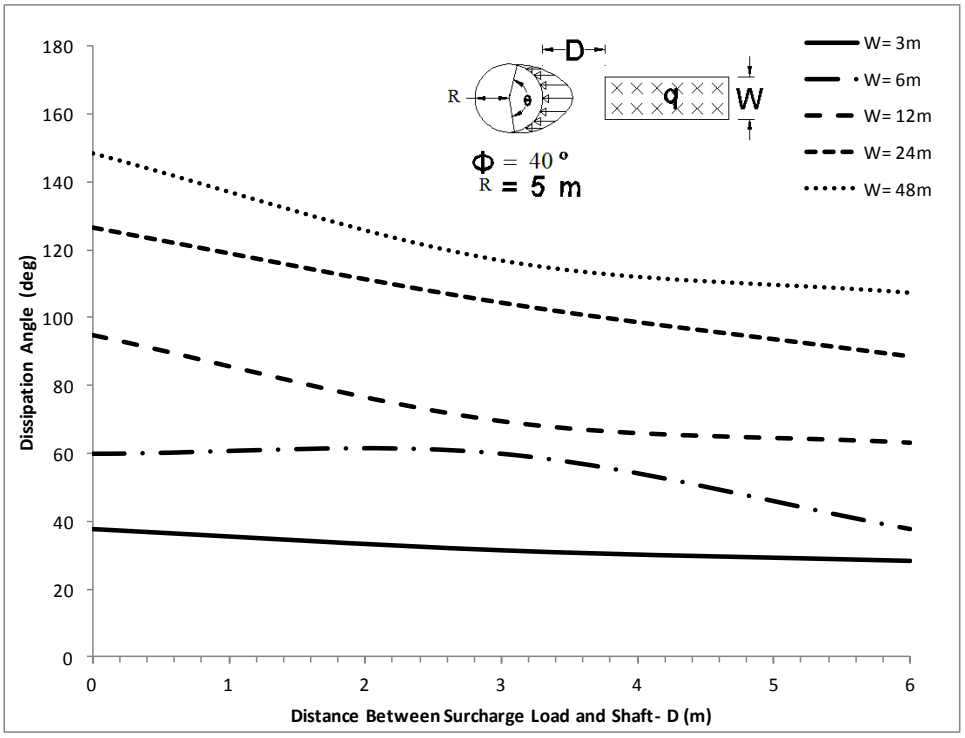

d

Figure 41. Variation of dissipation angles ,θ, for various ,R, values and soil types

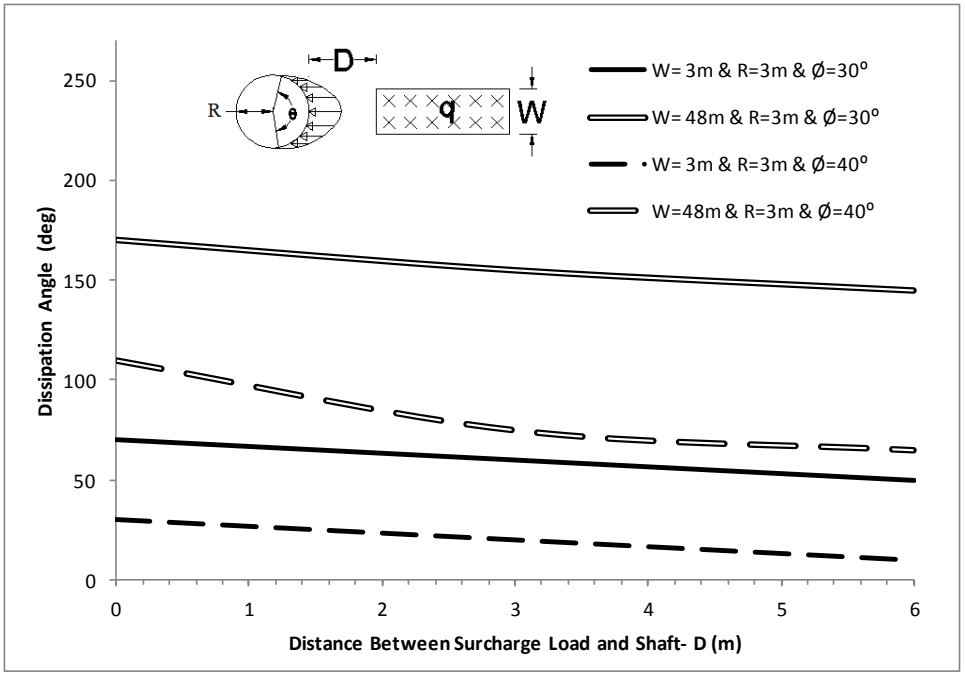

Figure 42. Effect of soil type on the dissipation angles for maximum surcharge pressures

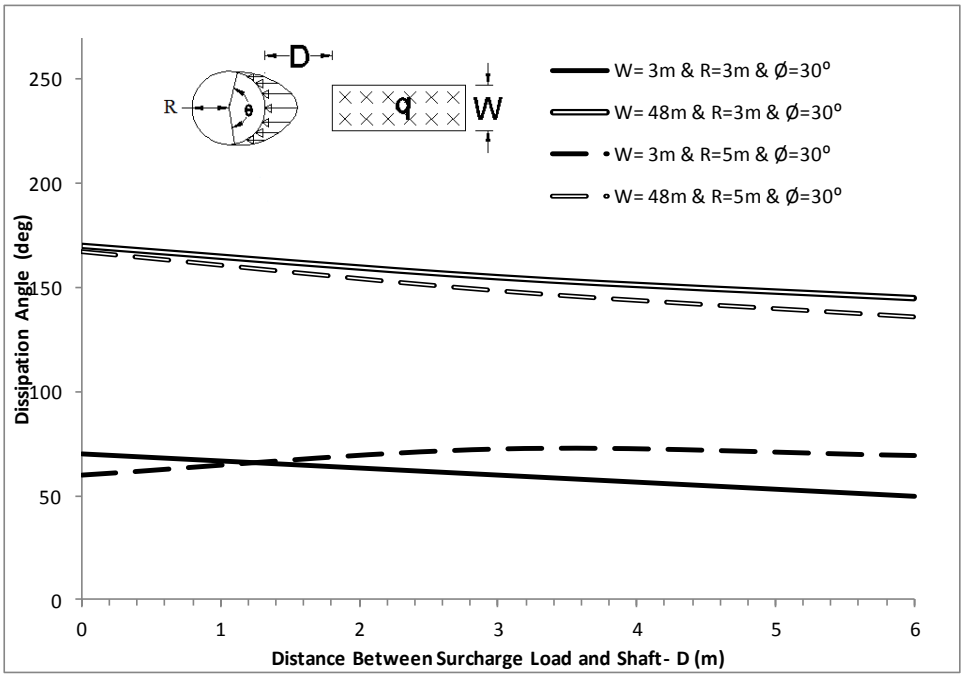

Figure 43. Effect of shaft radius on the dissipation angles for maximum surcharge pressures

5. Conclusions & Recommendations

5.1 Conclusions

Parametric numerical analyses were performed to investigate the interaction between secant pile wall circular shafts and surrounding soil/rock with the consideration of various practical aspects related to the design of these systems. Three-dimensional nonlinear finite element models were developed to conduct the parametric analyses using the commercial FE package, ABAQUS. Elasto-plastic soil behavior of retained soil and a non-linear soil-shaft interface were assumed in the analyses. The following conclusions can be drawn from this study.

1. The results showed that the calculated earth pressures for three soil types varied between at-rest and active conditions based on the type of soil and the depth of the point of interest. The earth pressures at shallow depths could be represented by an active distribution and those at large depths could be represented by an at-rest distribution.

2. The circular shaft exhibited compression ring behavior under balanced earth pressures and resultant wall movements were not large enough to reduce the lateral stresses from at-rest conditions to active conditions along the entire depth of shaft.

3. The stress concentration factors, which represent the stress variations caused by the excavation of holes on the shaft wall, were calculated for various (r/R) ratios. Stress concentration factors for compression (on top of the holes) were found to be a function of (r/R) ratios for curved surfaces of circular shaft walls.

4. The calculated stress concentration factors for tensile stresses (on the sides of the holes) were larger than the results of the theoretical solution (infinite plate with hole solution). However the calculated stress concentration factors for the compressive stresses were lower than the theoretical results except for very low (r/R) values. The results indicated that the solution devised for the case of holes on a plate is unconservative for the design of holes on circular shafts for most practical cases.

5. The interaction between the holes and their combined effect on the stress concentration factors were also studied. Compared to the shaft with one hole opening, the

shaft with two holes had lower compressive concentration factors but higher tensile concentration factors. It was also found that the values of stress concentration factors for the shaft with two holes were almost independent of the hole-to-hole distance, the distance between the hole and the shaft boundary.

6. Significant deviations from the expected compression ring behavior were observed when the pile toes were socketed into shallow bedrock. It was observed that the circular shafts that were installed on sloping bedrocks with inclination angles larger than 20 degrees experienced increased levels of compressive stresses as well as the additional tensile stresses that should be accounted for in the design stage.

7. It was seen that the width of the surcharged area, W, had a significant impact on the magnitude and distribution of surcharge-induced pressures on the shaft. The impact of W on the maximum surcharge induced lateral pressures on the wall was independent of the shaft radius, R. However, the surcharge distance from the shaft, D, and soil type were seen to have a significant impact on the effect of W on the maximum pressure.

8. The results showed that the distribution of surcharge induced lateral pressures on the wall differed from the theoretical distribution especially at larger depths. The results of analyses at larger depths exceeded the theoretical values. Thus, the use of theoretical pressure distribution at large depths is an unconservative assumption.

9. The results indicated that the maximum surcharge induced lateral pressure on the wall approached and exceeded the theoretical values as D increased. The results indicated that the calculated pressures were larger than the theoretical estimates at larger depths for all cases. However, it should be noted that the differences caused by D were small from a design perspective.

10. Both the soil type and shaft radius were shown to have significant impacts on the vertical distribution of surcharge pressures on the shaft wall. The maximum surcharge pressure on the shaft wall decreased with the increase of the shaft radius and soil friction angle $\emptyset$ as well.

11. The results show that the dissipation angle (θ), which is the angle to which the effect of surcharge pressures reach within the horizontal plane, was seen to be

significantly influenced by the soil type and width of surcharge. The radius of the shaft and the distance between the shaft and the surcharge were seen to have only a minor effect on the dissipation angles (θ).

5.2 Recommendations

Based on the outcomes of the present study, the following topics are suggested for future studies:

1. Small-scale physical modeling of a circular shaft in a soil box on a centrifuge to verify the conclusions made related to earth pressure on the shaft.
2. The monitoring of shaft stresses and earth pressures on a full scale circular shaft.
3. Numerical investigation of the effect of soil-to-rock stiffness ratios on stress distribution of a rock-socketed compression ring.
4. Numerical investigation of the effect of the construction process on the in-situ ground stresses prior to excavation.
5. Numerical investigation of the mechanics of circular shafts considering
    a. Circular shafts near buildings and the effect of stiffening the building embedment.
    b. Circular shafts near a moving slope.
6. Numerical investigation of the feasibility of partial reinforcement of circular shafts using embedded steel piles.
7. Numerical investigation of the impact of tieback use on the mechanical interaction between soil and shaft.

References

[1] M. U. Ergun, "Deep Excavations," *Electronic Journal of Geotechnical Engineering,* 2008.

[2] [Online]. Available: http://www.zakladani.cz/media/files/galleries/83/05-1386285416.JPG. [Accessed 5 January 2014].

[3] [Online]. Available: http://www.trevigroup.com/media/immagini/2329_2257_soil_improvement.jpg. [Accessed 5 January 2014].

[4] A. Turan, J. Weck and A. Chehadeh, "Behavior of two diaphragm wall circular shafts subjected to earth pressures," in *Deep Foundation Institute Middle East Conference*, Dubai, 2014.

[5] [Online]. Available: http://www.secantpile.com/themes/TekTracker/images/SecantPile_cp2.jpg. [Accessed 5 January 2014].

[6] [Online]. Available: http://www.secantpile.com/themes/TekTracker/images/secantpile_cs1b.jpg. [Accessed 5 January 2014].

[7] "Deephams Sewage Treatment Works," *New Civil Engineer,* pp. 22-24, 2010.

[8] K. Terzaghi, Theoretical Soil Mechanics, New York: John Wiley & Sons, 1943.

[9] V. Berezantzev, "Earth pressure on the cylindrical retaining walls," in *Conference on Earth Pressure Problems*, Brussels, 1958.

[10] E. Prater, "Examination of some theories of earth pressure on shaft linings," *Can. Geotech. J.,* vol. 14, no. 1, p. 91–106, 1977.

[11] E. D. Moor and M. Stevenson, "Evaluation of the performance of a multi-propped diaphragm wall during construction," in *Int. symposium on geotechnical aspects of underground construction in soft ground*, Balkema, 1996.

[12] I. H. Almadhoun, "Behavior of underground lined circular shafts.", Ph.D. thesis, The University of Arizona, United States, 1981.

[13] K.-Y. Kim, D.-S. Lee, J. Cho, S.-S. Jeong and S. Lee, "The effect of arching pressure on a vertical circular shaft," *Tunnelling and Underground Space Technology,* vol. 37, ISSN: 0886-7798, pp. 10-21, 2013.

[14] T. Tobar and M. A. Meguid, "Comparative evaluation of methods to determine the earth pressure distribution," *Tunnelling and Underground Space Technology,* vol. 25, no. 2, pp. 188-197, 2010.

[15] F. Liu, "Lateral earth pressures acting on circular retaining walls," *International Journal of Geomechanics,* vol. 14, no. 3, p. 4014002, 2014.

[16] M. Herten and M. Pulsfort, "Determination of spatial earth pressure on circular shaft constructions," *Granular Matter,* vol. 2, no. 1, pp. 1-7, 1999.

[17] A. Ghanbari and M. Taheri, "An analytical method for calculating active earth pressure in reinforced retaining walls subject to a line surcharge," *Geotextiles and Geomembranes,* vol. 34, ISSN: 0266-1144, pp. 1-10, 2012.

[18] S. Caltabiano, E. Cascone and M. Maugeri, "Seismic stability of retaining walls with surcharge," *Soil Dynamics and Earthquake Engineering,* vol. 20, no. 5, pp. 469-476, 2000.

[19] C.-D. Wang, "Lateral Force Induced by Rectangular Surcharge Loads on a Cross-Anisotropic Backfill," *Journal of Geotechnical and Geoenvironmental Engineering,* vol. 133, no. 10, pp. 1259 - 1276, 2007.

[20] C. Yoo and S.-B. Kim, "Performance of a two-tier geosynthetic reinforced segmental retaining wall under a surcharge load: Full-scale load test and 3D finite element analysis," *Geotextiles and Geomembranes,* vol. 26, no. 6, p. 460–472, 2008.

[21] K. Hatami and R. J. Bathurst, "Numerical Model for Reinforced Soil Segmental Walls under Surcharge Loading," *Journal of Geotechnical and Geoenvironmental Engineering,* vol. 132, no. 6, pp. 673-684, 2006.

[22] B. Virollet, C. Gilbert, Soletanche-Bachy, R. Deschamps and N. Construction, "Recent advances in large diameter diaphragm wall shafts," in *31st Annual Conference On Deep Foundations*, Washington, 2006.

[23] P. Makulsawatudum, D. Meckenzie and R. Hamilton, "Stress concentration at cross holes in thick cylindrical vessels," *Journal of Strain Analysis,* vol. 39, no. 5, pp. 471-481, 2004.

[24] S.Laczek, J.Rys and A.P.Zeilinski, "Load capacity of thick walled cylinder with a radial hole," *International Journal of Pressure vessels & Piping,* vol. 87, no. 8, pp. 433-439, 2010.

[25] G. Nihous, C. Kinoshita and S. Masutani, "Stress concentration factors for oblique holes in pressurized thick walled cylinders," *Journal of Pressure Vessel Technology,* vol. 130, no. 2, p. 21202, 2008.

[26] H. Li, R.Johnston and D.Meckenzie, "Effect of Autofrettage in Thick-Walled Cylinder With a Radial Cross-Bore," *Journal of Pressure Vessel Technology,* vol. 132, no. 1, p. 11205, 2010.

[27] C. Duncan, M. Donald and H.Robert, "Shakedown of a Thick Cylinder With a Radial Crosshole," *Journal of Pressure Vessel Technology,* vol. 131, no. 1, p. 11203, 2008.

[28] L. Xiao-li, Z. Dan-dan and S. Yuan-yuan, "A Method for Computing Embedded Depth in Rock of the Laterally Loaded Rock-socketed Piles," in *Electric Technology and Civil Engineering (ICETCE)*, Lushan, 2011.

[29] J. P. Carter and F. H. Kulhawy, "Analysis of Laterally Loaded Shafts in Rock," *Journal of Geotechnical Engineering,* vol. 118, no. 6, p. 839–855, 1992.

[30] L. Zhang, H. Ernst and H. H. Einstein, "Nonlinear analysis of laterally loaded rock-socketed shafts," *J. Geotech. Geoenviron. Eng.,* vol. 126, no. 11, pp. 955-968, November, 2000.

[31] L. C. Reese, "Analysis of laterally loaded piles in weak rock," *Journal of Geotechnical and Geoenvironmental Engineering,* vol. 123, no. 11, p. 1010–1017, 1997.

[32] Y. Arai, O. Kusakabe, O. Murata and S. Konishi, "A numerical study on ground displacement and stress," *Computers and Geotechnics,* vol. 35, no. 5, pp. 791-807, 2008.

[33] N. Thasnanipan, Z. Z. Aye, A. W. Maung, C. Submaneewong and T. Boonyarak, "Diaphragm wall support deep-excavations in bangkok," Seafco Public Company Limited, Thailand, 2000.

[34] E. GÜLER, " Methodology for Lining Design of Circular Mine Shafts in Different Rock Masses.", M.A. thesis, Middle East Technical University, Ankara, 2013.

[35] G. Auvinet-Guichard, J. F. Rodrı´guez-Rebolledo and J. L. Rangel-Nu´n˜ez, "Construction of deep tunnel shafts in Mexico city soft clays by the flotation method," *Acta Geotechnica,* vol. 5, no. 1, pp. 63-68, 2010.

[36] H. Sanada, T.Nakamura and Y.Sugita, "Mine-by Experiment in a deep shaft in Neogene sedimentary rocks at Horonobe,Japan," *International Journal of Rock Mechanics & Mining Sciences,* vol. 56, ISSN: 1365-1609, pp. 127-135, 2012.

[37] W. Yansen, Z. Chi, X. Libing and H. Xinggen, "Prediction and safety analysis of additional vertical stress within a shaft wall in an extra-thick alluvium," *Mining Science and Technology,* vol. 20, no. 3, pp. 0350-0356, 2010.

[38] L. S. Bryson and D. G. Zapata-Medina, "Finite-element analysis of secant pile wall installation," *Geotechnical Engineering,* vol. 163, no. 4, pp. 209-219, 2010.

[39] M.-K. Yeh and C.-Y. Chin, "Dynamic Response of Circular Shaft with Piezoelectric Sensor," *Intelligent Material Systems and Structures,* vol. 5, no. 6, pp. 833 - 840, 1994.

[40] R. Y. Liang and Mohammad Yamin, "Three-dimensional finite element study of arching behavior in slope/drilled shafts system," *Int. J. Numer. Anal. Meth. Geomech.,* vol. 34, no. 11, p. 1157–1168, 2010.

[41] L. Zhang, "Nonlinear analysis of laterally loaded rigid piles in cohesionless soil," *Computers and Geotechnics,* vol. 36, no. 5, p. 718–724, 2009.

[42] R. L. Handy, "The arch in soil arching," *J. Geotech. Engrg.,* vol. 111, no. 3, pp. 302-318, 1985.

[43] K. Yamamoto, A. V. Lyamin, D. W. Wilson, S. W. Sloan and A. J. Abbo, "Stability of a single tunnel in cohesive–frictional soil subjected to surcharge loading," *Can. Geotech. J.,* vol. 48, no. 12, p. 1841–1854, 2011.

[44] M. Iskander, D. Roy, S. Kelley and C. Ealy, "Drilled Shaft Defects: Detection, and Effects on Capacity in Varved Clay," *J. Geotech. Geoenviron. Eng.,* vol. 129, no. 12, pp. 1128-1137, 2003.

[45] D. Kruse, A. Basso, A. Le and T. Tan, "Exploratory finite element analysis (FEA) and conceptual design findings of large-diameter, segmentally lined shafts," *Mining Eng.,* vol. 63, no. 9, pp. 81-88, 2011.

[46] C. Dassault Systèmes Simulia, "ABAQUS/CAE 6.10-1," RI, 2010.

[47] Y. Shin and M. Sagong, "Ground pressure acting on cylindrical retaining wall of a shaft in soft ground," *Chinese Journal of Rock Mechanics and Engineering,* vol. 26, no. 2, pp. 3689-3696, 2007.

[48] R. C. K. Wong and P. K. Kaiser, "Design and performance evaluation of vertical shafts: rational shaft design method and verification of design method," *Canadian Geotechnical Journal,* vol. 25, no. 2, pp. 320-337, 1988.

[49] G. T. Houlsby and C. P. Wroth, "Direct solution of plasticity problems in soils by the method of characteristics," in *4th Int. Conf. on Numerical Methods in Geomechancis*, Edmonton, 1982.

[50] A. Drescher, "Limit plasticity approach to piping in bins," *Trans. J. Appl. Mech.,* vol. 50, no. 3, pp. 549-553, 1983.

[51] A. Drescher, "Kinematics of axisymmetric vertical slopes at collapse," *Int. J. Numer. Analyt. Meth. Geomech.,* vol. 10, no. 4, pp. 431-441, 1986.

[52] A. J. Jenike and B. C. Yen, "Slope stability in axial symmetry," in *5th Symp. on Rock Mechanics*, Pergamon, 1962.

[53] J. Hill and G. Cox, "Cylindrical cavities and classical rat-hole theory occurring in bulk materials," *International Journal For Numerical And Analytical Methods In Geomechanics,* vol. 24, no. 12, pp. 971 - 990, 2000.

[54] Y. Arai, O. Kusakabe, O. Murata and S. Konishi, "A numerical study on ground displacement and stress," *Computers and Geotechnics,* vol. 35, no. 5, pp. 791-807, 2008.

[55] M. Gunn, A. Satkunananthan and C. Clayton, "Finite element modeling of installation effects," in *ICE conference on retaining structures*, Cambridge, 1992.

[56] M. Gunn and C. Clayton, "Installation effects and their importance in the design of earth-retaining structures," *Geotechnique,* vol. 42, no. 1, pp. 137-141, 1992.

[57] G. Kutmen, "The influence of the construction process on bored piles and diaphragm walls: a numerical study," *M Phil thesis,* University of Surrey, 1986.

[58] E. D. Moor, "An analysis of bored pile/diaphragm wall installation," *Geotechnique,* vol. 45, no. 4, pp. 753-755, 1994.

[59] C. Ng and R. Yan, "Stress Transfer and Deformation Mechanisms around a Diaphragm Wall Panel," *Journal of Geotechnical and Geoenvironmental Engineering ,* vol. 124, no. 7, p. 638–648., 1998.

[60] S. Goto, M. Muramatsu, T. Sueoka, F. Saka, H. Yabe and H. Watanabe, "Ground movement earth and water pressures due to shaft excavations," in *int symposium on underground construction in soft ground*, Balkema, 1995.

[61] K. Ariizumi, T. Kumagai and A. Kashiwagi, "Behaviour of large-scale cylindrical earth retaining wall," in *int symposium on geotechnical aspects of underground construction in soft ground*, Balkema, 2000.

[62] M. Muramatsu and Y. Abe, "Considerations in shft excavation and peripheral ground deformation," in *int symposium on geotechnical aspects of underground construction in soft ground*, Balkema, 1996.

[63] H. Muller-Kirchenbauer, B. Walz and U. H. Klapperich, "Experimentelle und theoretische untersuchungen zum erddruck-problem auf radial symmetrische senkkasten und

schachte[R]," *Veroff. des Grundbauinstitutes der TU Berlin,* 1980.

[64] P. Lade, H. Jessberger, E. Makowski and P. Jordan, "Modeling of deep shafts centrifuge test," in *International conference on soil mechanics and foundation engineering*, Stockholm, 1981.

[65] D. Kim, M. Cha, D. Lee, K. Kim and I. Lee, "Earth pressure acting on vertical circular shafts considering arching effects in soils," *Tunell. Technol.,* vol. 12, no. 2, pp. 129-144, 2009.

[66] I. Lee, H. Moon, D. Lee, K. Kim and M. Choi, "Earth pressure of vertical shaft considering arching effect in layered soils," *Tunnell. Technol,* vol. 9, no. 1, pp. 49-62, 2007.

[67] W. J. M. Rankine, On the Stability of Loose Earth, London: The Royal Society, 1857.

[68] K. Paik and R. Salgado, "Estimation of active earth pressure against rigid retaining walls considering arching effects," *Geotechnique,* vol. 53, no. 7, pp. 643-653, 2003.

[69] K.-Y. Kim, D.-S. Lee, J. Cho, S.-S. Jeong and S. Lee, "The effect of arching pressure on a vertical circular shaft," *Tunnelling and Underground Space Technology,* vol. 37, ISSN: 0886-7798, pp. 10-21, 2013.

[70] R. J. Roark, W. C. Young and R. G. Budynas, Roark's formulas for stress and strain, New York: McGraw-Hill, 2002.

[71] J. Jaeger and N. Cook, Fundamentals of Rock Mechanics, London: Chapman & Hall, 1979.

[72] A. Nadai, Theory of flow and fracture of solids, New York: McGraw Hill, 1950.

[73] C. Coulomb, "Sur une application des regles maximis et minimis a quelques problems de statique, relatives a l'archetecture," *Acad Sci Paris Mem Math phys,* pp. 343-382, 1776.

[74] O. Mohr, "Welche Umsta¨nde bedingen die Elastizita¨tsgrenze und den Bruch eines Materials?," *Zeit des Ver Deut Ing,* p. 1524–1530, 1900.

[75] C. Dassault Systèmes Simulia, "Abaqus Reference Manual," RI, 2011.

[76] Y. Cheng and Y. Hu, "Active earth pressure on circular shaft lining obtained by simplified slip line solution with general tangential stress coefficient," *Chinese J. Geotech. Eng.,* vol. 27, no. 1, pp. 110-115, 2005.

[77] T. Fuji, T. Hagiwara, K. Ueno and A. Taguchi, "Experiment and analysis of earth pressure on an axisymmetric shaft in sand," in *International Conference on Centrifuge*, Singapore, 1994.

[78] S. Imamura, T. Nomoto, T. Fujii and T. Hagiwara, "Earth pressures acting on a deep shaft and the movements of adjacent ground in sand," in *International Symposium on Geotechnical Aspects of Underground Construction in Soft Ground*, Tokyo, 1999.

[79] B. Chun and Y. Shin, "Active earth pressure acting on the cylindrical retaining wall of a shaft," *South Korea Ground Environ. Eng. J.,* vol. 7, no. 4, pp. 15-24, 2006.

[80] J. T. Laba and J. B. Kennedy, "Reinforce earth retaining wall analysis and design," *Canadian Geotechnical Journal,* vol. 23, no. 3, pp. 317-326, 1986.

Vita

Ali Saleh Chehadeh was born in Abu Dhabi, United Arab Emirates, on 28th of August, 1990. He received his high school diploma from Khalifa Bin Zayed secondary school in Al Ain in 2008. He enrolled in and graduated from Abu Dhabi University (ADU) with a Bachelor's degree in Civil Engineering. Then, Ali joined the Master of Science in Civil Engineering in the American University of Sharjah (AUS). There he also worked as a Graduate Teaching Assistant from 2012 to 2014. Ali joined Technip - France Abu Dhabi on Sep. 2014 as an Offshore Structural Engineer.